

DANA: Dimension-Adaptive Neural Architecture for Multivariate Sensor Data

MOHAMMAD MALEKZADEH*, Imperial College London, UK

RICHARD CLEGG, Queen Mary University of London, UK

ANDREA CAVALLARO, Queen Mary University of London, UK

HAMED HADDADI, Imperial College London, UK

Motion sensors embedded in wearable and mobile devices allow for dynamic selection of *sensor streams* and *sampling rates*, enabling several applications, such as power management and data-sharing control. While deep neural networks (DNNs) achieve competitive accuracy in sensor data classification, DNN architectures generally process incoming data from a fixed set of sensors with a fixed sampling rate, and changes in the dimensions of their inputs cause considerable accuracy loss, unnecessary computations, or failure in operation. To address these limitations, we introduce a *dimension-adaptive pooling* (DAP) layer that makes DNNs flexible and more robust to changes in sensor availability and in sampling rate. DAP operates on convolutional filter maps of variable dimensions and produces an input of fixed dimensions suitable for feedforward and recurrent layers. Further, we propose a *dimension-adaptive training* (DAT) procedure for enabling DNNs that use DAP to better generalize over the set of feasible data dimensions at inference time. DAT comprises the random selection of dimensions during the forward passes and optimization with accumulated gradients of several backward passes. Combining DAP and DAT, we show how to transform existing non-adaptive DNNs into a *Dimension-Adaptive Neural Architecture* (DANA), while keeping the same number of parameters. Compared to existing approaches, our solution provides better average classification accuracy over the range of possible data dimensions at inference time and does not require up-sampling or imputation, thus reducing unnecessary computations. Experimental results on seven datasets (four benchmark real-world datasets for human activity recognition and three synthetic datasets) show that DANA prevents significant losses in classification accuracy of the state-of-the-art DNNs and, compared to baselines, it better captures correlated patterns in sensor data under dynamic sensor availability and varying sampling rates.

CCS Concepts: • **Human-centered computing** → **Ubiquitous and mobile computing systems and tools**; • **Computing methodologies** → **Neural networks**.

Additional Key Words and Phrases: Deep Neural Networks, Sensor Data Processing, Adaptive Sampling, Sensor Selection.

ACM Reference Format:

Mohammad Malekzadeh, Richard Clegg, Andrea Cavallaro, and Hamed Haddadi. 2021. DANA: Dimension-Adaptive Neural Architecture for Multivariate Sensor Data. *Proc. ACM Interact. Mob. Wearable Ubiquitous Technol.* 5, 3, Article 120 (September 2021), 27 pages. <https://doi.org/10.1145/3478074>

*Corresponding Author

Authors' addresses: Mohammad Malekzadeh, m.malekzadeh@imperial.ac.uk, Imperial College London, UK; Richard Clegg, r.clegg@qmul.ac.uk, Queen Mary University of London, UK; Andrea Cavallaro, a.cavallaro@qmul.ac.uk, Queen Mary University of London, UK; Hamed Haddadi, h.haddadi@imperial.ac.uk, Imperial College London, UK.

Permission to make digital or hard copies of all or part of this work for personal or classroom use is granted without fee provided that copies are not made or distributed for profit or commercial advantage and that copies bear this notice and the full citation on the first page. Copyrights for components of this work owned by others than ACM must be honored. Abstracting with credit is permitted. To copy otherwise, or republish, to post on servers or to redistribute to lists, requires prior specific permission and/or a fee. Request permissions from permissions@acm.org.

© 2021 Association for Computing Machinery.

2474-9567/2021/9-ART120 \$15.00

<https://doi.org/10.1145/3478074>

Proc. ACM Interact. Mob. Wearable Ubiquitous Technol., Vol. 5, No. 3, Article 120. Publication date: September 2021.

1 INTRODUCTION

Health and wellness applications [42, 43, 64] exploit motion sensors embedded in mobile and wearable devices to infer body movements and temporal changes in the physiological state of the wearer [8, 9, 20, 51]. For example, static acceleration (the magnitude and direction of the earth’s gravitational force) helps to recognize the wearer’s posture, whereas dynamic acceleration (changes in the velocity of the wearer) can be mapped to the wearer’s activity [56]. The time series generated by these motion sensors are processed over temporal windows and classified by deep neural networks (DNNs) [34, 55], which mostly process sensor data with pre-defined, fixed dimensions [25, 26, 28, 40, 45, 53, 63, 67, 69, 72]. Existing DNNs cannot reliably handle dynamic situations (e.g. when the sampling rate changes or some sensors are dropped), which are important for energy preservation [13, 35], privacy protection [39, 50] and fault tolerance [12, 41]. Moreover, DNNs are often trained on datasets collected from specific devices, but might be used for inference in a wider set of devices, with different combinations of sensors and sampling rates [32].

Previous works, which are mostly based on non-DNN-based approaches, have addressed either sensor selection [17, 19, 54, 68, 70, 73] or adaptive sampling rate [10, 23, 30, 47, 62], and dedicated a separate classifier for each feasible setting of available sensors [11, 24, 52]. The trade-off between classification accuracy and power consumption varies with changes in the sampling rate, the sensor streams used by the classifier, the type of the current activity, and the physical characteristics of the wearer [66]. Power-aware sensor selection may use a meta-classifier [70], or the prediction of future activities from the current one to deselect sensors that are not useful for future activities [19]. Alternatively, a graph model representing the correlation among sensors with a greedy approximation can be used for sensor selection [17], or a subset of sensors can be dynamically selected by minimizing an objective function that takes classification accuracy and the number of sensors as inputs [68].

Defining the minimum sampling rate that captures discerning frequency components in different human activities, for example, to minimize power consumption [13], is challenging [30] as the minimum required sampling rate varies across users, activities, and sensor positions. Khan *et al.* [30] show that the minimum sampling rate across activity recognition datasets varies between 22 and 63 Hz; with a 99% Kolmogorov-Smirnov similarity test [14]. It is therefore important to avoid aliasing to maintain the discernibility of activities characterized by higher frequencies [23, 62]. Yan *et al.* [66] propose to use a classifier with the highest sampling rate and then, after recognizing the current activity, switch to a lower sampling rate with another classifier and only monitoring whether the current activity changes or not. In order to lower power consumption, AdaSense [47] periodically detects changes in the current activity, by sampling data at higher frequencies, to check whether a lower sampling rate is suitable. To determine the best trade-off between power consumption and classification accuracy, Cheng *et al.* [10] find an optimal classification model as well as appropriate sampling rates using a continuous state Markov decision process that is only appropriate for training simple classifiers, such as softmax regression, and not applicable in training DNNs. Current DNN architectures for processing multivariate sensor data [25, 45, 53] cannot handle changes in the dimensions of their input without adding a data preprocessing stage to their pipeline. Thus, there is a lack of DNN architectures that can be trained for reliably and accurately handling variable data domains at inference time without any preprocessing stages.

In this paper, we introduce Dimension-Adaptive Neural Architecture (DANA), a unified, flexible and, more robust solution to variable sampling rates and sensor selection. At inference time, DANA works on any combination of sensors that were present at training time. Specifically, we introduce a dimension-adaptive pooling (DAP) layer that captures temporal correlations between consecutive samples and dynamically adapts to all feasible data dimensions. To enable DNNs, that use DAP, to generalize at inference time over the set of feasible dimensions, we propose a dimension-adaptive training (DAT) procedure, which incorporates dimension randomization and optimization with accumulated gradients. In each forward pass, DAT re-samples a batch of time windows to a new rate and may also randomly remove streams from some sensors. Then, gradients from multiple batches are

accumulated before updating the parameters. Combining DAP and DAT, we show how to transform existing DNNs into an adaptive architecture, with the same number of parameters and classification accuracy, and improving the inference time. In addition to allowing adaptive sampling rate and sensor selection with a unified solution, DANA enables the reduction of the computations to be performed according to the dimensions of the sampled data, which is desirable for power-constrained devices. We compare DANA with other existing baselines that use non-adaptive DNNs in terms of *the average classification accuracy* across a range of possible scenarios at inference time, where the more accurate a solution is on average, the more robust that solution is considered. Experimental results on seven datasets (four benchmark real-world datasets for human activity recognition and three synthetic datasets) show that DANA can maintain classification accuracy in dynamic situations where existing DNNs drop their accuracy, and better generalizes to unseen environments. Code and data to reproduce results are publicly available at <https://github.com/mmalekzadeh/dana>.

The paper is organized as follows. Section 2 covers the background and related work. In Section 3, we elaborate on how a DAP layer works, and in Section 4 we show how DNNs that use DAP can be efficiently trained using DAT. In Section 5 we evaluate DANA and compare it to non-adaptive DNNs and other baselines on real-world datasets. In Section 6, we provide experiments on three synthetic datasets where we control the correlation between two sensors and analyze the performance of DANA, compared to other baselines. Finally, in Section 7, we discuss some limitations and open directions in our work, for future studies.

As for the notation, we will use lower-case *italic*, e.g. x , for single-valued variables; upper-case *italic*, e.g. X , for single-valued constants; standard **bold** font, e.g. \mathbf{X} , for vector, matrices, and tensors; and standard blackboard bold, e.g. \mathbb{X} , for unordered sets. We use \times to separate the size of each dimension while \cdot denotes product.

2 BACKGROUND AND RELATED WORK

The architecture of a DNN is mainly defined by the type and number of layers, and how these layers are connected to each other [18]. The most common DNN architecture for sensor data classification consists of a convolutional neural network (CNN) [33] followed by a feedforward neural network (FNN) or a recurrent neural network (RNN) [25, 26, 40, 45, 53, 63, 67, 69, 72]. The main difference between FNNs and RNNs is that a FNN has no feedback connections. A feedback connection feeds the output of a neuron in a neural net, to the neuron itself. Every neuron in an RNN includes a feedback connection which helps to capture temporal correlations among consecutive samples.

A CNN is inherently adaptive to input data of variable dimensions [37] and is mainly used for feature extraction for the downstream task [18]. In computer vision, a prominent and motivational property of CNNs is that these layers can learn to be *invariant* to some changes (such as *translation*, *rotation*, or *scaling*) of objects in an image at inference time. For instance, it is well known that the convolution operation commutes with respect to the translation operation, meaning that when we convolve data \mathbf{X} with a filter \mathbf{F} , the output of is the same if (i) we convolve data and filter, and then translate the convolved output, or if (ii) we first translate data and, then convolve the translated data with the filter; i.e. $\tau(\mathbf{X} * \mathbf{F}) = \tau(\mathbf{X}) * \mathbf{F}$, where τ and $*$ denote the convolution and translation operations, respectively. Such a property of convolutional layers, alongside other architectural (e.g. max-pooling operation) and training (e.g. data augmentation) techniques, allow desired invariances in image processing to be satisfied [21, 29, 33, 37, 65]. These capabilities motivate our design of the DAP layer in Section 3 as well as the proposed DAT Section 4, which are aimed to force the ultimate model to be invariant to changes in sensor data characteristics, such as the sampling rate of sensor streams (similar to translation and scaling) and the *order* (or permutation) of available sensors (similar to rotation). In this paper, we put such changes in the sampling rate, order, and/or availability of sensor streams under the single umbrella of changes in the *dimensions* of sensor streams.

Features extracted by CNN to an FNN or an RNN improve the classification accuracy and provide better generalization compared to raw sensor data [6]. However, FNNs only work on fixed-dimension input data, and RNNs only accept a fixed number of streams, thus making the combination of CNNs with FNNs/RNNs non-adaptive to the changes in input dimensions. To address this limitation, a preprocessing stage can be added to the inference pipeline that up/down-samples data to a fixed rate or imputes dummy data to compensate for missing samples [3], but these solutions reduce classification accuracy and can even raise other challenges [49]. For example, when downsampling data, some discerning patterns are either removed or changed such that the resampled data will be miss-classified, which can be exploited by adversaries that take advantage of their knowledge about the used downsampling method to generate adversarial examples [49]. Our work eliminates the need for up/down-sampling the DNN's input at inference time, and thus less susceptible to such attacks.

Alternatively, to turn deep architectures based on CNNs and FNNs/RNNs adaptive to changes in input-data dimensions, a preferable solution is to include an adaptive layer between the CNN and the FNN/RNN. A global pooling layer [36] takes the maximum or average over each filter map of the CNN's output to make a one-dimensional vector whose length is equal to the number of the convolutional filter maps, and independent of the dimensions of these filter maps. The main drawback of global pooling is ignoring the inherent spatial structure of the data, and we show that it causes accuracy loss.

To mitigate the shortcomings of global pooling in visual object recognition, spatial pyramid pooling (SPP) [21] runs pooling on a pyramid that is created by hierarchically dividing a feature map into equally sized segments. SPP is supported by a weight-sharing mechanism for training CNN-FNN architectures on different image resolutions, and is used for transfer learning: the CNN part trained on the source dataset can be used with other FNNs on the target dataset [2]. SPP has promising results in image processing [71], but is not applicable to CNN-RNN architectures where recurrent layers, such as LSTMs [22], need two-dimensional inputs that preserve the temporal correlation among consecutive samples and across different sensor streams. Therefore, global or pyramid layers are not directly applicable to RNNs, which are often preferred for time-series classification [27]. Moreover, given DNNs for multivariate sensor data, there is no way for existing pooling layers to make them adaptive to temporal changes in input layer dimensions without changes that increase or decrease the number of trainable parameters and consequently may affect the model's accuracy.

A DNN that can process variable input dimensions should also be trained to produce accurate outcomes when the dimensions of its input can change. *Weight Averaging* [21] was proposed to build a single DNN by averaging the weights across multiple DNNs trained in parallel across different settings, which is also used in federated learning where the goal is to collaboratively train a shared model across different users [7]. Similarly, in meta-learning, the goal is to train a model across a large number of different tasks [15]. *Reptile* [44] is a meta-learning algorithm that uses the average parameters of multiple DNNs, each trained on a different task, as input to the optimizer for updating the DNN's parameters, instead of directly using the gradients of the loss function.

Unlike existing adaptive pooling layers [21, 36], our proposed DAP layer considers the temporal correlations in data as well as the absence of some of the sensors. This is particularly important as RNNs are more efficient in processing temporal data than FNNs [45, 69, 72]. Moreover, the proposed DAT resolves the need for weight sharing via training multiple DNNs, providing a faster and more accurate training algorithm, compared to the existing ones [7, 21, 44]. Finally, unlike the methods proposing multimodal fusion [11, 52], our solution resolves the need for training and deploying multiple DNNs which is particularly important for applications running mobile and wearable devices with limited power and processing resources.

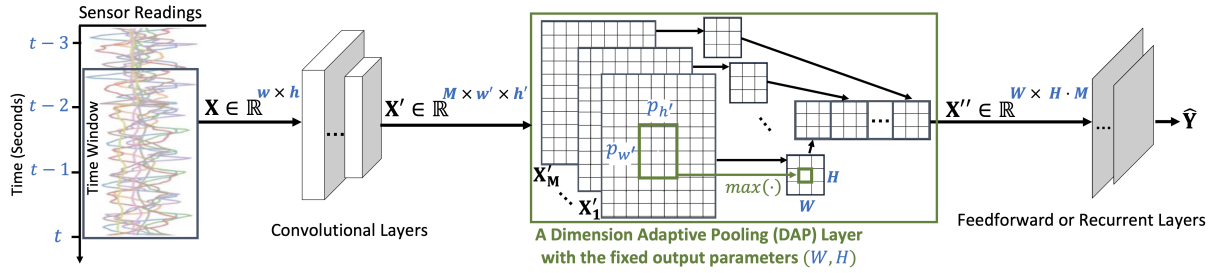


Fig. 1. A DAP layer enables a DNN performing classification on input data of variable dimensions. At time t , a window \mathbf{X} of dimensions $w \times h$ is received by the DNN. The number of *streams*, h , depends on the number of available sensors, while the number of *samples*, w , per each stream depends on the current sampling rate (in Hz) and the length of time window (in seconds). For example, a 2.5-seconds time window of 50 Hz data generated by three 3-dimensional motion sensors (*e.g.* accelerometer, gyroscope, and magnetometer of a smartwatch) has dimensions of $w = 125$ and $h = 3 \cdot 3 = 9$. Convolutional layers process \mathbf{X} , then DAP is applied to the M outputs of the last convolutional layer \mathbf{X}' . DAP uses an adaptive kernel of size $p_w' \times p_h'$ that is calculated based on DAP's chosen parameters, (W, H) , and the dimensions of CNN's outputs, $w' \times h'$. Data of fixed dimensions, \mathbf{X}'' , is provided for the following feedforward or recurrent layers that output the classification's result $\hat{\mathbf{Y}}$.

3 DIMENSION-ADAPTIVE POOLING (DAP)

We propose the DAP layer to handle situations where one or more sensors may dynamically be deselected at inference time. The flexibility of DAP aims not only to make DNNs adaptive to changes in the dimension of data, but also to allow efficiently training the DNN such that it provides reliable performance across several combinations of data dimensions.

Considering a multivariate time-series (see Fig. 1), let \mathbf{X} be a time window of dimensions $w \times h$ where w is the number of samples, which depends on the sampling rate and the length of the time window, and h is the number of sensor streams. Particularly in our case, motion sensors have three spatial axes (x, y, z), thus $h = 3 \cdot s$, where s is the number of available sensors. Thus, if a sensor is not available, or deselected, then \mathbf{X} will have 3 fewer streams. In real-world situations, when a sensor is available it produces measurement in all three axes, and it is not usual that, for example, an accelerometer only produces measurement on only one axis or two of its three axes. There might be situations where the produced data for an axis is noisy or wrong, *e.g.* due to hardware issues, but we still receive a sensor stream in that axis. We emphasize that we do not investigate distinguishing between faulty or normal sensor streams in this paper, and we only consider the availability or not availability of sensor streams.

A DNN can cope with inputs of variable dimensions by using a convolutional layer as the input layer. A two-dimensional convolutional layer slides M fixed-sized *filters* across the input data, and computes the dot products between each filter's entries and the data at the current position of the filter, resulting in M two-dimensional filter maps (\mathbf{X}' 's in Fig. 1). In a stack of convolutional layers, the dimensions of the CNN's output, $w' \times h'$, mainly depend on the dimensions of the input data¹, $w \times h$.

The outputs of a CNN's last layer are in a three-dimensional shape², $w' \times h' \times M$, which is not suitable as direct input to a FNN or RNN. The usual practice is to reshaped such three-dimensional data into one-dimensional data of size $w' \cdot h' \cdot M$ for FNNs (by stacking all $h' \cdot M$ vectors of length w' next to each other) or two-dimensional data $w' \times h' \cdot M$ for RNNs (by stacking all M matrices of length $w' \cdot h'$ next to each other). For specific details, see

¹Design parameters such as the number of convolutional filters, M , size of the filters, the chosen padding mode, and the stride length of the filters are fixed at inference time.

²Note that in our notation, \times separates the size of each dimension while \cdot denotes product.

ReshapeLayer in TensorFlow library [1]. However, these typical DNNs can cope only with input data of fixed dimensions. One cannot simply use existing layers to make DNNs, which are proposed for processing sensor time-series, adaptive to the sampling rate and sensor selection without imposing any architectural changes. For instance, the single-dimensional data produced by SPP [21] is not appropriate for RNNs where the input must be provided in two dimensions: consecutive samples and parallel streams. DAP addresses the aforementioned limitations without enforcing assumptions on the DNN architecture to be used. DAP builds upon the global and pyramid pooling ideas and aims to map the outputs of dimensions $w' \times h' \times M$ into data whose dimensions are consistent with the next FNN/RNN layer. The size of the pooling filters in DAP is not limited to be square, hence it generalizes existing adaptive layers [21, 36].

Algorithm 1 shows the functionality of the DAP layer for DNNs processing motion sensor data³. Let (W, H) be the pre-specified hyper-parameters for pooling all the M feature maps into an output X'' of single dimension of size $W \cdot H \cdot M$ (if the next layer is FNN) or two dimensions $W \times H \cdot M$ (if the next layer is RNN). DAP first calculates the pooling parameters $(p_{w'} = \lfloor \frac{w'}{W} \rfloor, p_{h'} = \lfloor \frac{h'}{H} \rfloor)$ for the received inputs. It then, for every segment of size $(p_{w'}, p_{h'})$ on the received input, chooses the maximum value to create a the output which aims to be of fixed-dimensions (W, H) . For larger data dimensions, the pooling parameters adaptively cover a larger segment of the data and for smaller data dimensions the pooling parameters will shrink appropriately. Hence, DAP always produces an output of fixed dimensions.

As an example, consider a CNN-RNN and $s = 3, w' = 128, h' = 9, W = 16, H = 3, M = 32$. The maximum of every 8 consecutive samples among all 3 axes of each sensor will be chosen for the output, thus producing X'' with dimensions $16 \times 3 \cdot 32$. If we deselect two sensors and choose a sampling rate half of the original, this means $w' = 64$ and $h' = 3$, then DAP adaptively keeps the output fixed, by choosing the maximum of every $8/2 = 4$ consecutive samples of each axis of the only available sensor.

The input of DAP has dimensions $w' \times h'$, which can be variable at training and inference time; whereas the output of DAP, X'' , is fixed and includes $W \cdot H \cdot M$ values. The first inner loop in Algorithm 1 (lines 9-11) handles situations when one or more sensors are unavailable. Depending on the value of H , we may need to replicate some of the existing streams to satisfy fixed-sized outputs. For a DAP layer with $W = 16, H = 9$, and 3 sensors, the possible situations are as follows.

(1) All the sensors are available ($h' = 9$), thus $a = 0$ (in line 8 of Algorithm 1) and the algorithm skips the loop (Lines 9-11).

(2) One sensor is unavailable ($h' = 6$), thus $a = 1$ and the loop fills the gap by *vertically concatenating* a copy of the data from available sensors to the second dimension of the input data. Therefore Z will have $h' = 12$ streams and Line 12 truncates Z on its second dimension to ensure that its second dimension satisfies $H = 9$.

(3) Two sensors are unavailable ($h' = 3$), thus $a = 2$ and the algorithm fills the gap by *vertically concatenating* a copy of the data from the only available sensor two times. So, we will again satisfy $H = 9$.

Note that Line 12 guarantees that, in case of concatenating data to Z , the number of streams in data never exceeds H , and it has a neutral effect when $h' = H$. The next two loops, in Lines 16-29, perform the pooling operation over the consecutive segments of Z .

Following our example, in each iteration we consider a segment of data including w'/W samples and h'/H streams. For example, if $w' = 96$ then the maximum of every 6 consecutive samples of each sensor stream (e.g. the accelerometer's x-axis) is calculated and appended to Q (Line 27). If we only change H to 3, instead of 9, a will be zero, thus no concatenation happens. On the other hand, every segment of data includes $6 \cdot 3 = 18, 6 \cdot 2 = 12$, or $6 \cdot 1 = 6$ samples if all three, two, or only one sensor(s) are (is) available, respectively. Therefore, DAP adaptively changes the size of pooling segments to ensure that the output dimensions are fixed. Also note that, in Lines 16-29, the first loop runs on the first dimension W and the second loop on the second dimension H : this order

³ $\lfloor \cdot \rfloor$ denotes floor, $\lceil \cdot \rceil$ denotes ceiling, and $\lceil \cdot \rceil$ denotes rounding to the nearest integer.

Algorithm 1 – Dimension Adaptive Pooling (DAT). A layer to be located between the last convolutional layer and the first feedforward/recurrent layer in a DNN. DAT is designed to make DNN flexible to changes in sampling rate and sensor availability. A flexibility that is further utilized in Algorithm 2 (DAT) for training and making the DNN robust to such changes at inference time, in terms of the average classification accuracy.

```

1: Input:  $X'$ : filter maps received from a CNN,  $(W, H)$ : the fixed output parameters.
2: Output:  $X''$ : input to the next layer.
3:  $M, w', h' = \text{dimensions\_of}(X')$ 
4:  $X'' = \{\}$ 
5: for  $m = 1$  to  $M$  do
6:    $V = X'[m]$ 
7:    $Z = \text{copy\_of}(V)$ 
8:    $a = \max(\lceil (H - h')/3 \rceil, 0)$ 
9:   for  $i = 1$  to  $a$  do
10:     $Z = \text{concatenate\_vertically}(Z, V)$ 
11:   end for
12:    $Z = Z[0 : w', 0 : \max(h', H)]$ 
13:    $p_{w'} = w'/W$ 
14:    $p_{h'} = h'/H$ 
15:    $Q = \{\}$ 
16:   for  $i = 1$  to  $W$  do
17:     for  $j = 1$  to  $H$  do
18:        $r_1 = \lfloor i \cdot p_{w'} \rfloor$ 
19:        $r_2 = \lfloor (i + 1) \cdot p_{w'} \rfloor$ 
20:       if  $a=0$  then
21:          $c_1 = \lfloor j \cdot p_{h'} \rfloor$ 
22:          $c_2 = \lfloor (j + 1) \cdot p_{h'} \rfloor$ 
23:       else
24:          $c_1 = \lfloor j \cdot \lfloor (a + 1) \cdot p_{h'} \rfloor \rfloor$ 
25:          $c_2 = \lfloor (j + 1) \cdot \lfloor (a + 1) \cdot p_{h'} \rfloor \rfloor$ 
26:       end if
27:        $Q = \text{append}(Q, \max(Z[r_1 : r_2, c_1 : c_2]))$ 
28:     end for
29:   end for
30:    $X'' = \text{append}(X'', Q)$ 
31: end for

```

preserves the temporal correlation between consecutive samples, which is necessary for DNNs that use recurrent layers.

4 DIMENSION ADAPTIVE TRAINING (DAT)

Although a DNN using DAP can accept input of any dimensions, it should be properly trained for being adaptive to changes, otherwise, its classification accuracy will be low when the input's dimensions change. In particular, we cannot anticipate which sensors are available at inference time, and consequently, an adaptive model should be ready for such changes not only in the sampling rate but also in the type and order of receiving

Algorithm 2 – Dimension Adaptive Training (DAT). To train A DNN that is made flexible to changes in sampling rate and sensor availability by DAP layer in Algorithm 1. During training, DAT randomly encounters the DNN with a range of feasible data dimensions at inference time and imitatively updates the DNN with the accumulated gradients of multiple feasible data dimensions.

```

1: Input:  $\mathbb{D}$ : training datasets,  $\Theta$ : trainable parameters,  $E$ : number of epochs,  $\mathbb{U}$ : a subset of all feasible dimensions,
    $B$ : number of batches used in each optimization round,  $K$ : size of each batch.
2: Output:  $\Theta$ : optimized parameters.
3: for  $e = 1$  to  $E$  do
4:   while not feeding the DNN all data in  $\mathbb{D}$  do
5:      $\mathcal{G} = 0$ 
6:     for  $b = 1$  to  $B$  do
7:        $\mathbb{X} = \text{generate\_random\_batch}(\mathbb{D}, K)$ 
8:        $\mathbb{X} = \text{dimension\_randomization}(\mathbb{X}, R)$ 
9:        $\hat{\mathbb{Y}} = \text{forward\_pass}(\Theta, \mathbb{X})$ 
10:       $\mathcal{G} = \mathcal{G} + \text{Gradients}(\text{Loss}(\mathbb{Y}, \hat{\mathbb{Y}}))$ 
11:     end for
12:      $\Theta = \text{optimizer}(\Theta, \mathcal{G})$ 
13:   end while
14: end for

```

sensor streams. To this end, we leverage the capability of CNNs (discussed in Section 2) in being invariant to changes in the scale and location of observed patterns in the data. To cover this important requirement, we need a training procedure for adaptive DNNs that encounters the model with such potential changes in the type of sensor streams, that could happen at inference time, to make the model less sensitive to the changes in the scale, type, and order of incoming sensor streams.

The *multi-size training* procedure [21] for images trains in parallel two DNNs with different dimensions but with shared weights. This multi-size training is problematic with sensor data because of the large variety of possible training situations. For example, 10 sampling rates (e.g. 5, 10, 15, . . . , 50 in Hz) and the 7 possible combinations of 3 sensors lead to 70 DNNs to train. To overcome this challenge and provide a reasonable, converging training strategy, we propose dimension adaptive training (DAT). In DAT, we train a single DNN, and therefore there is neither a need for weight sharing nor for choosing a specific set of data dimensions. DAT comprises of two main ideas: *dimension randomization* and *optimization with accumulated gradients* (Fig. 2). The DAT process works by training the DNN on input data of several randomly selected dimensions and sensor orders. In this way, DAT forces the model to leverage the underlying correlations between data streams coming from different motion sensors and learn dimension- and order-invariant features. Specifically, DAT randomly encounters convolutional filters with sensor patterns that appear in different locations and with different scales. Then, by accumulating and averaging the gradients computed on B such random observations, DAT guides these convolutional filters toward achieving the capability of being invariant to potential changes at inference time. For efficiency, the data is processed in batches of input data that has the same dimension. The details of DAT are shown in Algorithm 2.

Each round of optimization includes two steps. First, a random batch, \mathbb{X} , of K time windows of the highest available sampling rate is generated from the dataset. For batch number, b , the available sensors are chosen randomly and a random sampling rate is chosen with data downsampled using bilinear interpolation. All the time

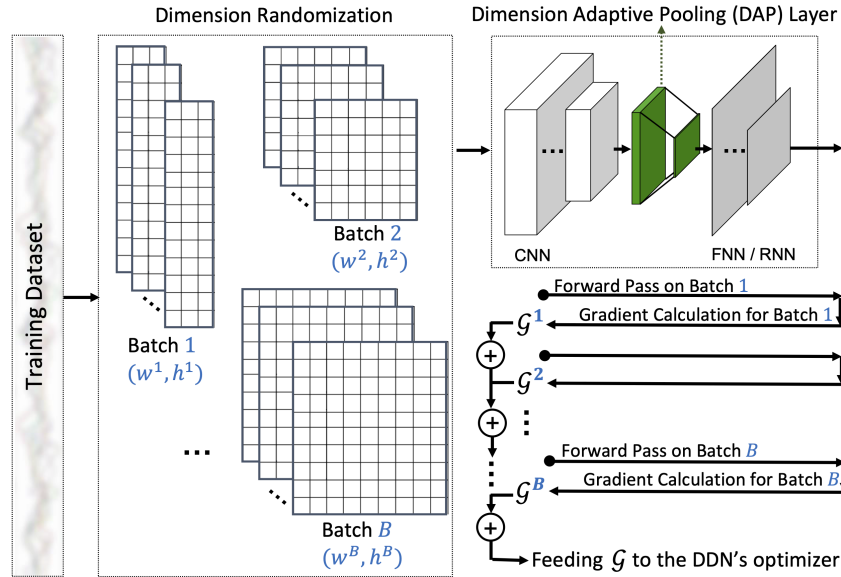


Fig. 2. Overview of each iteration in DAT (Algorithm 2). B batches of time windows are randomly generated from a training dataset. All time windows in each batch are transformed into the same randomly chosen dimensions $w^b \times h^b$, thus samples within each batch have the same dimension while samples among batches have different dimensions. Every batch is iteratively fed into DNN and the corresponding gradients with respect to the current loss value are accumulated into \mathcal{G} . After computing the gradients of all B batches, the parameters of the DNN are updated based on $\mathcal{G} = \sum_{i=1}^B \mathcal{G}^i$.

windows in batch b have the same dimensions⁴ $w_b \times h_b \in \mathbb{U}$. Considering an example where the possible sampling rates range from 6 Hz to 50 Hz, instead of considering all the 45 possible cases, we only choose a subset \mathbb{U} , for instance including 8 sampling rate $\{6, 12, 18, 25, 31, 37, 43, 50\}$ (in Hz). In the epoch e , $dimension_randomization()$ in Line 8 randomly and uniformly chooses, for instance $B = 4$ of this 8 sampling rates without replacement. Second, a forward pass is performed on batch b giving a vector of predictions, $\hat{\mathbb{Y}}$. we calculate the average loss value (e.g. categorical cross-entropy) of the predictions compared with the true labels, \mathbb{Y} , and its gradients, corresponding to the Θ , is accumulated into \mathcal{G} . These two stages are repeated B times, then using the accumulated gradients, \mathcal{G} , the parameters the DNN, Θ , are updated at once.

As DNNs tend to forget previously learned information upon learning from new data, updating Θ immediately after computing losses for each batch of data causes catastrophic forgetting [16], in which the DNN may repeatedly forget how to perform classification on the previously trained dimensions. We show that the combination of dimension randomization and gradient accumulation not only helps DAT to prevent catastrophic forgetting but also to converge better.

It is worth noting that the gradient accumulation in DAT is similar but a different concept than the typical method of keeping track of gradient *momentum* in stochastic gradient descent [48]. In a momentum-based optimization, a scaled version of the gradients used in the previous round is added to the gradients of the current round. Thus, at each round, the DNN's parameters are updated based on the current gradients and the history of

⁴Note that, the key point of efficiently training DNNs on GPUs is in eliminating loops by matrix multiplications that force all samples in each batch, b , to have the same dimensions in a forward pass.

Table 1. Details of the four real-world datasets used in our evaluations. For all datasets, the original sampling rate is 50 Hz.

| Dataset | Characteristics | | | |
|-----------------|--|---|-----------------|-----------------------------|
| | Sensors | Type of Activities | Number of Users | Device Position |
| UCI-HAR[4] | Accelerometer Gyroscope | {Sit, Stand, Walk, Lie, Stairs-Down, Stairs-Up} | 30 | Chest Mounted |
| MobiAct[61] | | {Sit, Stand, Walk, Jog, Stairs-Down, Stairs-Up} | 61 | Trousers Front Pocket |
| MotionSense[38] | Accelerometer Gyroscope Magnetometer | {Sit, Stand, Walk, Jog, Bike, Smoke, Drink, Eat, Talk, Type, Write, Stairs-Down, Stairs-Up} | 24 | Trousers Front Right Pocket |
| UTwente[57] | | | 10 | Right Wrist |
| | | | | |

the past gradients. On the other hand, DAT is a procedure for computing the required gradients in a single round, hence we can use DAT and a momentum-based optimization, such as Adam [31], together.

5 EVALUATION

5.1 Evaluation Setup

Since existing DNN architectures require fixed-dimension input data, the only DNN-based alternative to our proposed DANA is to add a data preprocessing stage to the inference pipeline that up/down-samples data to the fixed sampling rate and imputes synthetic data to compensate for unavailable sensor streams. As discussed in Section 1 and 2, our solution offers competitive advantages over this alternative, such as eliminating the need for preprocessing as well as adapting the required computations at inference time while having the same size as existing DNNs. In the following, we focus on *classification accuracy* as the main evaluation criterion for our comparisons. In particular, we measure the classification accuracy of DANA and the other alternative (which we refer to it as the *original* model) across a range of possible scenarios. In each scenario, the more a DNN maintains its average accuracy, despite changes in the dimension at inference time, the more robust the DNN is considered.

We evaluate DANA on four public datasets of human activity recognition: *UCI-HAR* [4], *UTwente* [57], *MobiAct* [61], *MotionSense* [38]. We show how to transform three state-of-the-art CNN-FNN/RNN architectures for sensor-based human activity recognition [25, 45, 53] into a DANA, and discuss how DAP works with and without using DAT. We also evaluate the advantages of DANA at training time, compared with three other training procedures: *standard*, *weight averaging* [21], and *Reptile* [44], and at inference time compared with two alternatives baselines: *imputation* and *resampling* with and without *data augmentation*. Finally, we perform an experiment across two datasets to show the generalization of DANA.

UCI-HAR [4] is a widely used dataset [25, 45, 53, 72] of 30 users performing 6 activities. Accelerometer and gyroscope data were collected by a smartphone worn on the waist. Data from 21 users are used for training and that of the other 9 users for testing purposes [4].

UTwente [57] includes data of 10 users performing 13 activities. We use accelerometer, gyroscope, and magnetometer data collected from the device on the (right) wrist. We divide the dataset into 80% training and 20% validation.

MobiAct [61] and **MotionSense** [38] include accelerometer and gyroscope data from 61 and 24 users, respectively, with a smartphone in the pocket of the trousers. We use the data from the 6 activities in common among the two datasets. In the MobiAct dataset, for each activity, we keep 2/3 of trials for training and 1/3 of them for validation [38]. We use the entire MotionSense dataset for test purposes and do not use it in the training. For all experiments, we use a time window $T = 2.56$ seconds (i.e. a maximum of 128 samples per window) [25, 45, 53]. Table 1 shows the details of the datasets, including the activity classes.

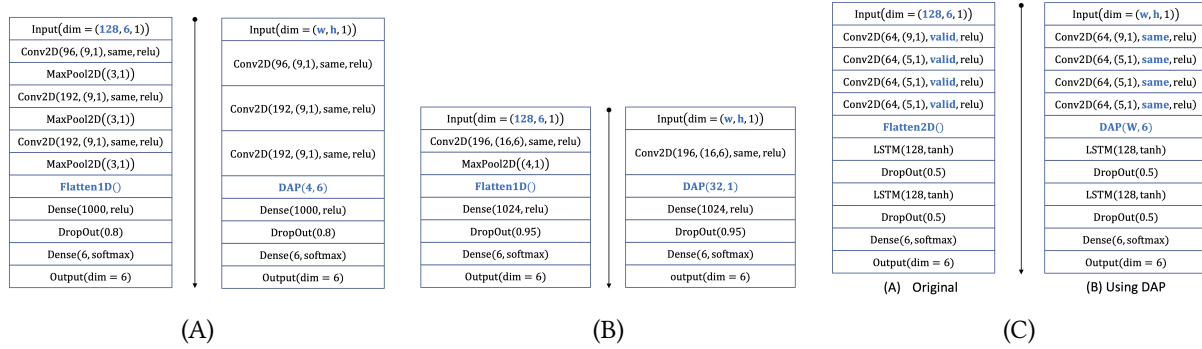


Fig. 3. The original DNNs (left plots) proposed in (A) [53], (B) [25], and (C) [45], versus their DANA version (right plots). The differences between each pair of DNNs are shown in blue bold font. We use TensorFlow’s naming conventions [1].

5.2 Transforming a DNN into DANA

Fig. 3 compares the original architectures proposed in the related work [25, 45, 53] and our modified version using DAP. A 2D convolutional layer is shown by $\text{Conv2D}(n, (k_1, k_2), padding, activation)$ where n is the number of neurons, (k_1, k_2) is the size of the 2D kernel used by each neuron; if *padding* is *same*, the output and the input of the layer have the same dimensions, otherwise if it is *valid* then the output has $k_1 - 1$ and $k_2 - 1$ values fewer than the number of inputs in the first and second dimensions, respectively; *activation* shows the nonlinear activation function applied to the output of the layer; $\text{Dense}(n, activation)$ shows a fully-connected feedforward layer; $\text{LSTM}(n, activation)$ shows a recurrent LSTM [22] layer; $\text{MaxPool2D}((p_1, p_2))$ shows a 2D maximum pooling layer that outputs the maximum value of each window including $p_1 \cdot p_2$ data points; $\text{Dropout}(q)$ applies Dropout [59] with probability q that randomly sets the output of a neuron to 0 during each forward pass in training time; $\text{FlattenXD}()$ reshapes its inputs into 1D or 2D outputs.

To transform a non-adaptive DNN into a DANA, we only use a single DAP layer, instead of “maximum pooling” layers, with appropriate pooling parameters (W, H) , and instead of “valid” padding, we use “same” padding. Thus, we can keep the total number of trainable layers and parameters exactly the same as the original DNN.

5.3 Original DNNs versus Their DANA Version

To ensure the comparison is fair among all DNNs, we use the same number of epochs (1,000), early stopping patience (100 epochs), and batch size (128). We also use the same optimizer as reported in the corresponding works: for the models with FNN, Adam [31], and for the models with RNN, RMSProp [60]. We run each model 10 times and report the mean and standard deviation for classification accuracy.

Table 2 compares the classification accuracy for each DNN architecture with that architecture using DAP instead of their standard maximum pooling. Although we set (W, H) such that the transformed architecture has the same model size as the original DNN; it is possible to choose any other values getting a larger or smaller size DNN. Here, two settings are considered for evaluations. (i) *Validate*: where the whole training dataset is used for training, and the test dataset is used for validation. Thus, each DNN is trained on the training dataset and the validation dataset is used to check the accuracy of the model after each epoch. This is the setting that is used by other works re-implemented [25, 53]. (ii) *Test*: where 10% of the training dataset is randomly chosen as the validation set and the rest (90%) is used as the training set. Here, the test dataset is used to evaluate the best trained DNN on the validation set.

Table 2. Classification accuracy of three benchmark DNNs (see Figure 3) on UCI-HAR dataset, the original non-adaptive models proposed in [53], [25], and [45], versus the corresponding adaptive model with a DAP layer. Notice that we set (W, H) such that the transformed architecture has the same model size as the original DNN. The results, where the sampling rate is fixed to 50Hz and both sensors are available, show that making these DNN flexible, by our proposed DAP layer, does not lead to a loss in the DNN's accuracy.

| Architecture | Size | DNN $[(W, H)]$ | Setting | Accuracy (%) | |
|----------------|-----------------|-----------------|-----------------|-----------------|---------|
| | | | | Mean \pm STD | Maximum |
| CNN-FNN | 5,114,014 | [53] | <i>validate</i> | 93.85 \pm .49 | 94.51 |
| | | | <i>test</i> | 91.92 \pm .97 | 93.14 |
| | | with DAP(4,6) | <i>validate</i> | 93.73 \pm .84 | 95.39 |
| | | | <i>test</i> | 91.88 \pm 1.1 | 93.04 |
| CNN-FNN | 6,448,714 | [25] | <i>validate</i> | 93.80 \pm .59 | 94.78 |
| | | | <i>test</i> | 92.75 \pm .73 | 94.02 |
| | | with DAP(32,1) | <i>validate</i> | 93.89 \pm .41 | 94.57 |
| | | | <i>test</i> | 92.57 \pm .60 | 93.65 |
| CNN-RNN | 457,030 | [45] | <i>validate</i> | 94.13 \pm .53 | 95.25 |
| | | | <i>test</i> | 91.66 \pm 1.3 | 93.45 |
| | | with DAP(4,6) | <i>validate</i> | 94.69 \pm .31 | 95.32 |
| | | | <i>test</i> | 94.07 \pm .39 | 94.77 |
| | | with DAP(8,6) | <i>validate</i> | 94.82 \pm .34 | 95.32 |
| | | | <i>test</i> | 93.47 \pm .81 | 94.33 |
| with DAP(16,6) | <i>validate</i> | 94.69 \pm .48 | 95.18 | | |
| | <i>test</i> | 93.19 \pm .59 | 94.02 | | |
| with DAP(32,6) | <i>validate</i> | 94.74 \pm .33 | 95.32 | | |
| | <i>test</i> | 93.23 \pm .92 | 94.70 | | |

Table 2 shows that for all three architectures the classification accuracy of the adaptive version is either slightly improved or almost the same as the original DNN, in both *validate* and *test* settings. This suggests that the DAP layer does not lead to a loss in accuracy while providing the desirable adaptivity, that is further utilized by DAT. The CNN-RNN model has 10 times fewer parameters than the FNN but has a better classification accuracy. The CNN-RNN with DAP significantly improves accuracy in the *test* setting, thus suggesting that DAP helps the model to better generalize to the test data. RNNs are also flexible on their first dimension, which is the number of samples per stream. Thus, unlike FNNs, we can use DAP layers having different pooling parameters for the first dimension while keeping the rest of the architecture the same. Changing the pooling parameters leads to slightly different accuracies, which can be used as part of a fine-tuning pipeline for DNN models but would not be possible with FNNs.

To see the performance of the DNNs and DANA on another dataset, we evaluate existing DNNs (without fine-tuning) on UTwente, which is a different dataset from those datasets used in the original papers of the implemented DNNs. Table 3 shows that the CNN-RNN architecture [45] has better generalization than the other two CNN-FNN architectures. The model using DAP maintains a comparable accuracy.

We see that transforming a DNN into DANA does not change the trainable parameters of the DNN, whereas using other global pooling or SPP layers would require a change in the size of the FNN/RNN layers and consequently the number of trainable parameters of the original DNN. As an experiment, to measure the effect of using

Table 3. Classification accuracy (%) of three benchmark DNNs on the UTwente dataset (that does not use in any of the original papers [53], [25], and [45]). Results show that the DNN using RNN layers [45] offers better generalization than the other two DNNs using FNNs. Similar to Table 2, we see that the adaptive version of [45], using our DAP layer, achieves a similar, and even slightly better, classification accuracy.

| DNN | Size | Ref. | Accuracy | |
|---------|------------|----------------|-----------|---------|
| | | | Mean±STD | Maximum |
| CNN-FNN | 7,425,021 | [53] | 59.20±9.6 | 76.99 |
| | 12,878,417 | [25] | 78.85±6.2 | 88.01 |
| | | [45] | 93.68±.36 | 94.55 |
| CNN-RNN | 556,237 | with DAP(8,9) | 94.35±.37 | 95.16 |
| | | with DAP(16,9) | 94.64±.40 | 95.40 |

the global average pooling layer [36], we run a similar experiment on CNN-RNN [45] with UCI-HAR. The model size is reduced from 457K to 293K, but also the classification accuracy (%) reduced from $94.13 \pm .53$ to $78.6 \pm .81$.

It should be noted that this experiment only aims to show that using a DAT layer does not degrade the accuracy, and not to show that using a DAT layer we can achieve better accuracy in a fixed-dimensions scenario. As we show in other experiments, the main advantage of DANA is keeping high accuracy in variable-dimensions scenarios. As the *validate* setting is what is considered in other works [25, 53], where they report the *best accuracy* that corresponding DNN can achieve on the dataset, for the rest of the experiment we use the *validate* setting for fair comparisons. Note that as we do not tune any hyper-parameters and do not change the size of trainable parameters in all DNNs, similar relative results are achieved in the *test* setting. But, unlike the *validate* setting which has only one instance (*i.e.* a training set and a validation set), the *test* setting could be biased because there are many possible instances depending on the randomly chosen 10% validation set.

5.4 Changes in Sampling Rate and Sensor Availability

Fig. 4 compares the original and DANA version of the DNN proposed by [45], as CNN-RNN performs better. First, using the original DNN, the model can only be trained and validated on data of fixed dimensions. To see how the original model performs if we change the sampling rate, we keep the weights and parameters of the original model and use them on a version using DAP (lines with a cyan cross and red plus). Second, we have a DNN version that only uses DAP during the training but is only trained on a fixed sampling rate (lines with yellow and blue triangles). Finally, we have the DANA version (the line with green square) which not only uses DAP, but it also uses DAT with $B = 4$ and $\mathbb{U} = \{6, 12, 18, 25, 31, 37, 43, 50\}$ (in Hz).

Although DANA version slightly reduces the accuracy on the specific sampling rates the other DNN versions were trained on (34Hz and 50Hz), it considerably outperforms the other DNN versions across the whole range of sampling rates, where the accuracies of other DNNs drops quickly when moving away from their pre-defined settings. Because the best accuracy of DANA occurs at 34 Hz, for this reason, we trained other DNNs on this specific sampling rate, thus suggesting that DAT is consistent in its performance while being adaptive.

To see the effect of sensor selection, Fig. 6 shows the replication of the previous experiment (in Fig. 4) in different sensor-selection scenarios. Here, DANA is trained to account for the possibility of deselecting (or missing) sensors, and the other lines are the same as in Fig. 4 where the training only considers sampling rate selection and does not account for sensor selection. During training, 50% of the time, DANA is trained on both sensors, and 50% of the time with one of accelerometer or gyroscope (randomly chosen with equal probability). The values of B and \mathbb{U} are the same as Fig. 4.

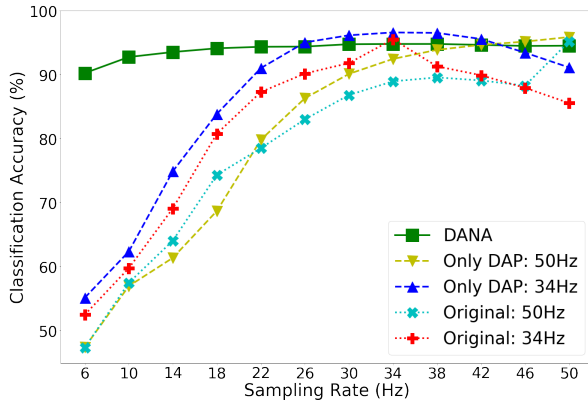


Fig. 4. Classification accuracy of CNN-RNN [45] on UCI-HAR dataset for varying sampling rates (but fixed available sensors). DANA keeps the accuracy above 90% in all situations; due to DAT training. Only sing a DAP layer, without training with DAT, achieves a similar performance to the original DNN. We evaluated the original DNN, on all fixed-sampling rates from 6Hz to 50Hz, and found 34Hz proposing the maximum test accuracy.

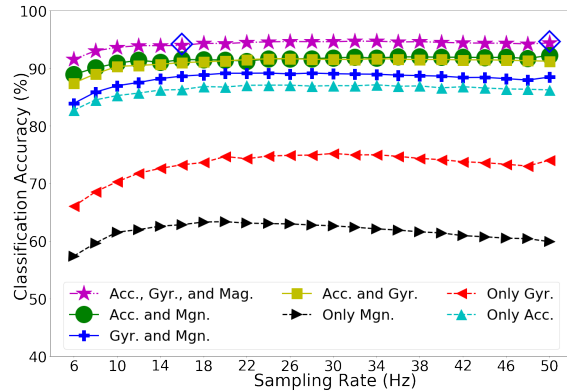


Fig. 5. Classification accuracy of DANA with DAT for both dimensions on UTwente dataset with the DANA version of the CNN+RNN proposed by [45]. The two points, shown by \diamond at 16 Hz and 50 Hz, show the accuracy of the original DNN when trained on these fixed sampling rates.

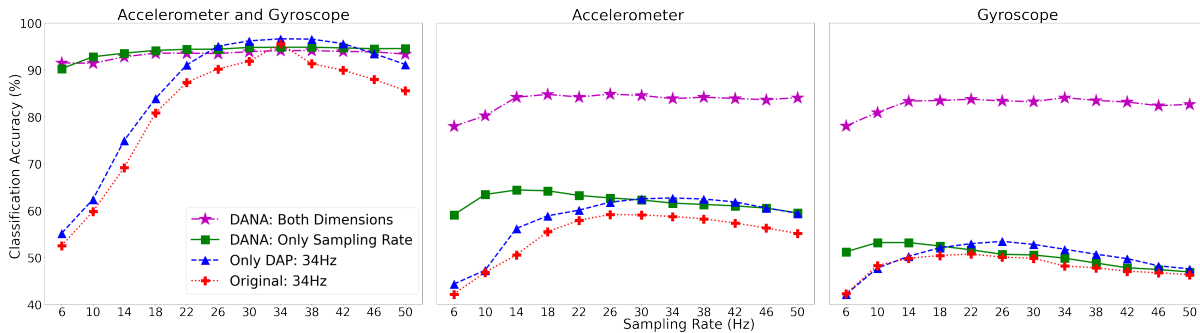


Fig. 6. Classification accuracy of CNN-RNN [45] on UCI-HAR dataset with a variable sampling rate and sensor availability. When both sensors are available (left), versus when only the accelerometer (middle) or gyroscope (right) is available. Overall, with DAT for both dimensions (\star) performs much better than DANA with DAT for only sampling rate (\blacksquare).

Fig. 6 (left) shows that the adaptivity to the sensor selection is not associated with a large penalty when all sensors are present. Fig. 6 (middle) shows that when the gyroscope is deselected, DANA maintains its accuracy around 85% while the accuracy of other DNNs falls rapidly to around 60%. Similarly, Fig. 6 (right) shows that when the accelerometer has deselected the accuracy for DANA remains around 85% while other DNNs fall to 50% or less. It is interesting that while for other DNNs deselecting accelerometer data causes more accuracy loss than deselecting gyroscope, the type of the deselected sensor has a reduced effect on DANA.

In Fig. 5 we make the CNN-RNN model adaptive to both sampling rate and sensor availability using DAP and DAT on UTwente, and we achieve similar accuracy to the original model. Note that, while original DNNs are not

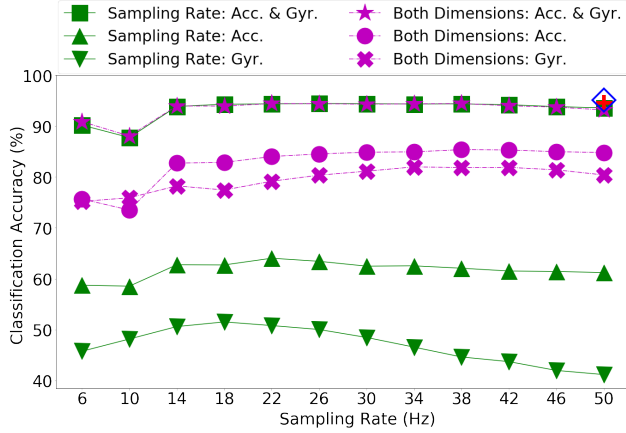


Fig. 7. Classification accuracy of DANA on UCI-HAR using a CNN-FNN [53]. The data points + and \diamond at 50 Hz refer to Table 2 accuracies.

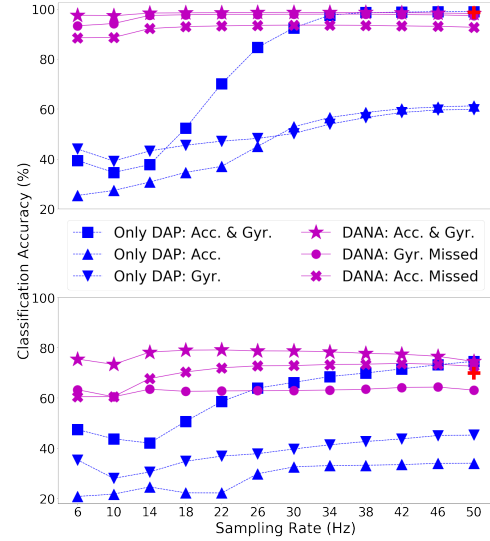


Fig. 8. Classification accuracy of a CNN+RNN [45] trained on MobiAct [61] and tested on MotionSense [38]. The single data point shown by + at 50 Hz refers to the accuracy achieved with the original DNN in Table 4.

Table 4. Accuracy (%) of CNN-RNN architecture proposed in [45] trained on the MobiAct training dataset and validated on the MobiAct and MotionSense test datasets.

| DNN | MobiAct | MotionSense | |
|----------|---------|-------------|-------------------|
| | | Normalized | Pseudo-Normalized |
| Original | 98.64 | 69.87 | 44.16 |
| Only DAP | 98.91 | 74.65 | 49.65 |
| DANA | 98.18 | 74.60 | 47.97 |

reliable when the data dimensions change, DANA provides at least 55% accuracy across $7 \cdot 45 = 315$ feasible data dimensions.

Fig. 7 compares the accuracy for different versions of a CNN-FNN proposed by [53]. The accuracy of DANA, trained on both variable sampling rates and variable sensors, remains high for a variety of sampling rates. When one of two sensors is deselected, the accuracy loss is much smaller than the one obtained from training only on variable sampling rates, with fixed sensors. The accuracy loss for this generalization is small when compared with the single points that show the situations where the DNN is only trained on a fixed sampling rate with all sensors present without and with DAP, respectively.

5.5 A Cross-Dataset Experiment

We train three versions of the CNN-RNN proposed in [45] on MobiAct and test them on MotionSense. We follow two settings: *normalized*, where we normalize the MotionSense data to zero mean and unit standard deviation,

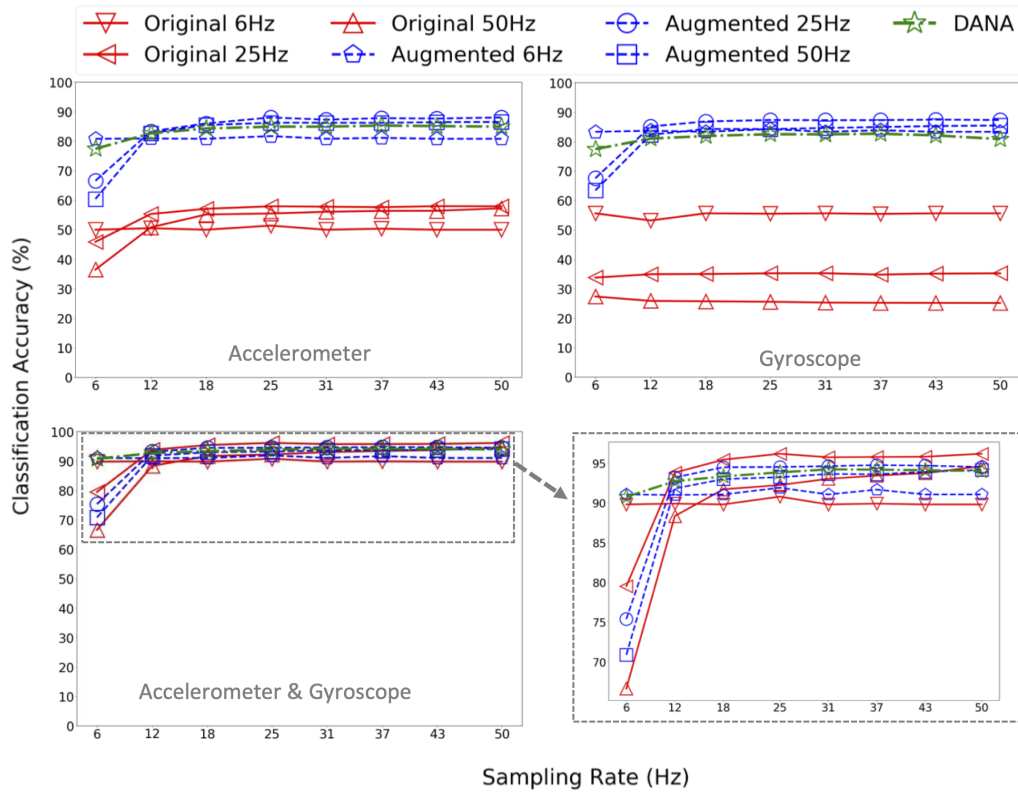


Fig. 9. Comparing DANA with two baselines approaches using CNN-RNN [45], where the non-adaptive DNN is trained on the UCI-HAR dataset as it is (*Original*), or via an extended version of UCI-HAR dataset by making a copy of every sample for all possible combinations of sensors availability (*Augmented*). Each non-adaptive DNN is trained on three fixed sampling rates (6, 25, and 50Hz). For situations at inference time where incoming data has a different sampling rate, we use down/up-sampling to the fixed sampling rate used in training time.

and *pseudo-normalized*, where we use the MobiAct statistics to normalize the MotionSense data to mean zero and unit standard deviation. The latter is standard practice as when streaming data, the mean and standard deviation are not known in advance. All three models have the same number of parameters and were trained under the same training setting.

Table 4 shows that DANA generalizes better on the test dataset, in terms of accuracy, by about 5 percentage points. This result confirms that for the corresponding datasets, using DAT to make a DNN adaptive helps to achieve a more accurate model in an unseen environment⁵. Although the DANA version has a slightly lower accuracy than the one using only DAP, DANA is the only reliable model when the dimensions of the input data change (see Fig. 8). Thus, while DANA shows a bit smaller accuracy than the original DNN on MobiAct, this will considerably pay off when DANA is used in dynamic settings which we have shown in the results of the previous experiments.

⁵MobiAct was collected with a Samsung Galaxy S3 in the right or left pocket of the trousers. MotionSense was collected with an iPhone 6s in the front, right pocket of their trousers.

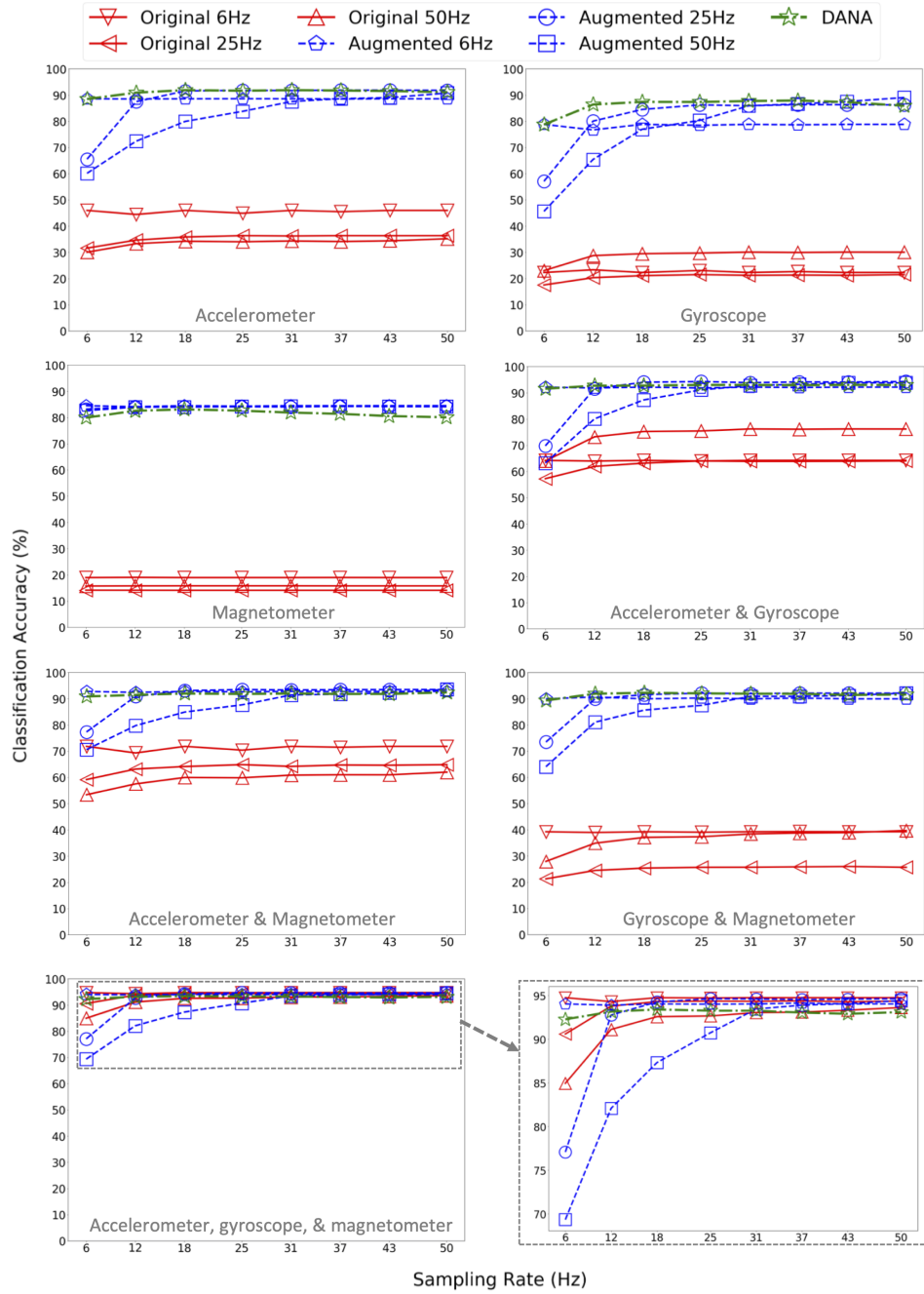


Fig. 10. Comparing DANA with two baselines using CNN-RNN [45]. Everything is similar to the experiment in Fig. 9, except the dataset that is UTwente that contains three sensors.

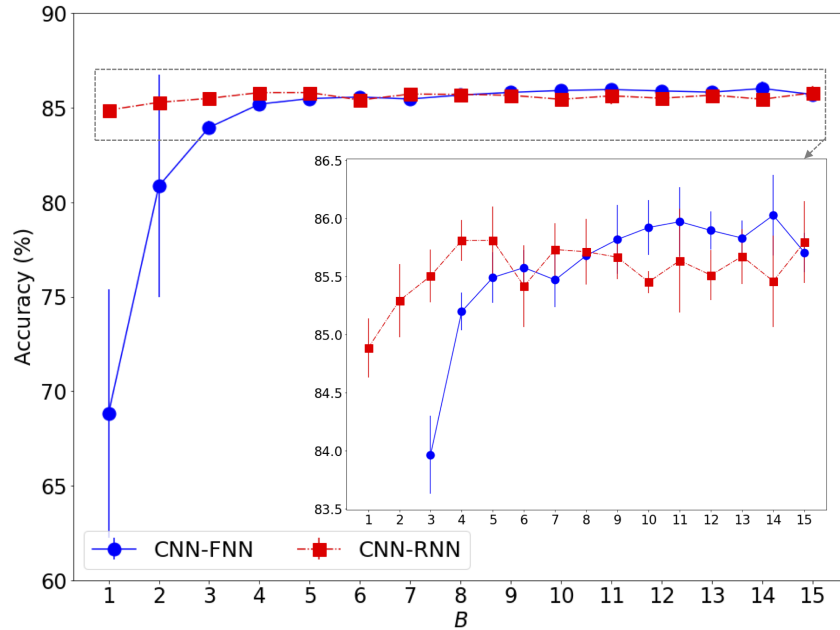


Fig. 11. Effect of the size of resampling batches B on UCI-HAR with CNN-RNN [45]. Each point is the average and each segment shows the standard deviation for 5 runs.

5.6 Comparison with Baselines

As we discussed earlier on in Section 5.1, an alternative baseline to DANA is to take the original model, and every time the sampling rate is changed, we fix the problem by re-sampling data to the original sampling rate, and if some sensors are missing or deselected, we impute synthetic or dummy data, *e.g.* inserting zeros, using the *mean values* for each stream computed on the training dataset, or just *copying* the data of available sensor(s). Moreover, when choosing the copying strategy, one can also use an *augmented* training dataset by making a copy of the data for every possible combination of sensors availability. For example, with 3 sensors, we augment the training dataset with 6 other time windows per each sample time window in the training dataset. For example, assume that we only have accelerometer data available at inference time, among three possible sensors. And, thus we add sample time windows to the training dataset that includes accelerometer data copied two more times to cover the other two unavailable sensors. Notice that, the training time for the *augmented* case is 2^s times the training time for the DANA (where s is the number of sensors).

Fig. 9 and 10 compares DANA with these baselines. We see that DANA can train a single model that outperforms the original model across all 56 settings, and also outperforms the augmented case for lower sampling rates (while remaining competitive for larger sampling rates). Note that the augmented baseline needs a longer training time and also does not reduce the computations when sampling rate changes or some sensors are unavailable or deselected. These results show that DANA can capture the correlation, or information redundancy, between different sensor streams. For example, when the original models miss a sensor or two, their accuracies considerably fall, because they are not able to substitute the missed information using the available ones. But DANA keeps the accuracy at the same level as the augmented one, while it does not need to endure the difficulties of the augmented one at the training and inference time.

Table 5. Comparison of different training methods for turning a DNN adaptive to changes in the input data dimensions. Accuracy denotes the classification accuracy and times (average time per each training epoch) are in the unit of seconds (s).

| Dataset DNN Model Optimizer | UCI-HAR [4] | | | | | | UTwente [57] | |
|-----------------------------------|---------------------|-----------------|---------------------|-----------------|---------------------|-----------------|---------------------|-----------------|
| | CNN+FNN [53] | | CNN+RNN [45] | | | | CNN+RNN [45] | |
| | Adam | | RMSProp | | Adam | | Adam | |
| Method | Accuracy (%) | Time (s) | Accuracy (%) | Time (s) | Accuracy (%) | Time (s) | Accuracy (%) | Time (s) |
| Standard | 69.94±6.08 | 4.24±.29 | 86.21±.11 | 6.03±.17 | 86.98±.21 | 5.55±.15 | 87.02±.51 | 14.24±.44 |
| WeightAvg | 85.90±.25 | 5.63±.13 | 86.61±.19 | 6.54±.10 | 87.02±.21 | 6.07±.14 | 88.14±.99 | 15.03±.45 |
| Reptile | 85.73±.25 | 5.50±.11 | 15.91±2.25 | 6.23±.10 | 86.87±.26 | 5.96±.19 | 87.87±.74 | 15.01±.43 |
| DAT (Ours) | 85.74±.20 | 3.68±.08 | 87.12±.13 | 5.58±.15 | 87.50±.11 | 5.43±.15 | 88.91±.59 | 13.30±.57 |

5.7 Comparison with Other Training Approaches

We explore the impact of the value of the training hyper-parameter B on the accuracy. Fig. 11 shows, for both CNN-FNN and CNN-RNN, the classification accuracy is comparable for RNN for $B \geq 4$ (whereas FNN cannot be trained with these values), and in general it suggests setting a $B \geq 5$.

Table 5 shows that DAT either outperforms or achieves comparable accuracy to other methods in several settings, and is always faster in training. The training approaches we compare with are *Standard*, the typical training procedure that includes a forward pass on a batch of data to calculate loss value, following with a backward pass to update model parameters based on the gradients; *WeightAvg* [7, 21], when each of the B copies of the model is trained on a dedicated batch of data using the *Standard* approach, and then the average parameter values of updated B copies will be used to update the central model; and *Reptile* [44], which performs the same procedure as *WeightAvg*, except the last step when the average parameters of B copies, each trained on a different batch of data, is fed to the chosen DNN optimizer, instead of the typical gradients of the loss function, to update the central model. The value of B is fixed to 5 for all experiments in Table 5. The *time* shows the average training time per each iteration over the whole training dataset (*i.e.* one epoch). Note that, DAT is not sensitive to the chosen optimizer, or dataset, or DNN architecture. Also, Reptile works with Adam (that is mentioned in the original paper [44]), but it cannot be useful with the RMSProp optimizer.

6 CONTROLLED EXPERIMENTS

Here, we design a controlled experiment to better understand the capabilities of DANA, compared to other available solutions. We generate a synthetic five-class dataset that simulates two motion sensors in a way that we can adjust the correlation between patterns observed in two sensors. Thus, we provide evaluations in three different settings of correlation: low, moderate, and high correlation.

6.1 Synthetic Dataset

When looking at real-world data of motion sensors, we observe that there are not only meaningful correlations between axes x, y , and z of a sensor, but, more importantly, there are also considerable correlations between the same axes of different sensors. For example, in UTwente[57] dataset the average absolute of *Pearson correlation coefficient*⁶ between accelerometer and gyroscope, accelerometer and magnetometer, and gyroscope and magnetometer are $0.25 \pm .20$, $0.34 \pm .29$, and $27 \pm .21$ respectively. Similarly, for UCI-HAR[4] we observe $0.21 \pm .17$ as the average absolute of Pearson correlation coefficient between accelerometer and gyroscope. It is important to note that there definitely are other types of non-linear correlations between the streams of two sensors. While

⁶A measure of linear correlation between two sets of data with the absolute value between 0 and 1; see https://en.wikipedia.org/wiki/Pearson_correlation_coefficient.

such non-linear dependencies are not easy to measure, non-linear machine learning models, such as DNNs, can capture and utilize them.

Motivated by these facts, we generate a five-class dataset of six-variate time series (simulating two motion sensors), while: (1) we control the correlation between two time series, and (2) we assign a class (*i.e.* label) to each time series such that samples within the same class share some similarities while having some differences with samples of other classes. In the following, we briefly explain the ideas we applied for this purpose. The code and complete instructions, including all the details and parameters used for generating these synthetic datasets, are published at <https://github.com/mmalekzadeh/dana>.

First, for axis x of two sensors $S1$ and $S2$ (the same process is followed for other axes y and z), and for class $c \in \{0, 1, 2, 3, 4\}$, we sample $S1_x$ and $S2_x$ from correlated Gaussian distributions with mean 0 and variance $\sigma_c^2 \in \{0.6, 0.7, 0.8, 0.9, 1\}$ in three settings of correlations $\rho = \{low : 0.01, moderate : 0.58, high : 0.89\}$, such that: $S1_x \sim \mathcal{N}(0, \sigma_c^2)$ and $S2_x \sim \mathcal{N}(\rho x_i^2, (1 - \rho^2)\sigma_c^2)$. Considering width $w = 50$, we repeat sampling for $i \in \{1, \dots, 50\}$, that with our choices of value for ρ , gives us two time series with exact mutual information $I(S1_x; S2_x) = -\frac{w}{2} \log(1 - \rho^2) = \{low : 0.01, moderate : 0.20, high : 0.80\}$. This is a standard technique for generating controllable correlated vectors [5, 46]. However, this is not enough, because in the current $S1_x$ and $S2_x$ we only have point-wise correlations between two sensors and no temporal correlation between sample points in each sensor. Thus, as the next step, we add some temporal patterns observed in real-world time series [58]. In particular, we add three *periodic*, one *trend*, one *smoothing* (via moving average), and one *white noise* components to each time-series $S1_x$ and $S2_x$ generated in the previous step. We set the characteristics of these additional components such that they have meaningful contributions to the base Gaussian signals but do not entirely dominate them. For the low correlations setting, we add these components with different characteristics to each sensor, but for the high correlations setting, we add these components with similar characteristics to each sensor. For the moderate correlations setting, we add a mixture of components with similar and different characteristics to each sensor. Also, to make our classification task non-trivial, the characteristics of each component are chosen differently across different classes.

To build intuition, we plot some sample examples of the generated data in Fig. 12. For each setting (of low, moderate, and high correlation), we generate 4,000 time windows of dimensions ($w = 50, h = 6$) as the training set; 900 time windows per class. Similarly, we generate 1,000 time windows as the test set; 100 time windows per class. We cannot compute the mutual information for the ultimate time series, because they include other non-Gaussian components, but we can compute Pearson correlation coefficient. For each setting, the average absolute of Pearson correlation coefficient is: (1) $0.15 \pm .10$ for the low correlation setting, (2) $0.54 \pm .11$ for the moderate correlation setting, and (3) $0.82 \pm .05$ for the high correlation setting; which they are consistent with our initial correlations considered for different settings. In the training and test set of each class, the characteristics of all described components are the same, except the noise component (to keep training and test samples of each class similar, while having a slight difference between them).

6.2 Experimental Results

We consider a very simple version of the architecture proposed in [45] (see Figure 3) including 2 convolutional layers followed by 1 LSTM layer, where each layer has only 5 neurons. In total, this neural network has less than 2K trainable parameters. For each setting of *low*, *moderate*, and *high* correlation between two sensors, we compare: (1) the original model with standard training using two baselines, and (2) the DANA version of the model including DAP layer with DAT training. As our two baseline approaches, for the original model to deal with the missed (or deselected) sensor at inference time, we consider: (1) *original_mean* where we use the mean values obtained from the training dataset for filling instead of the missed sensor, and (2) *original_copy* where we duplicate the data of available sensor for the missed sensor. Moreover, to deal with changes in the sampling

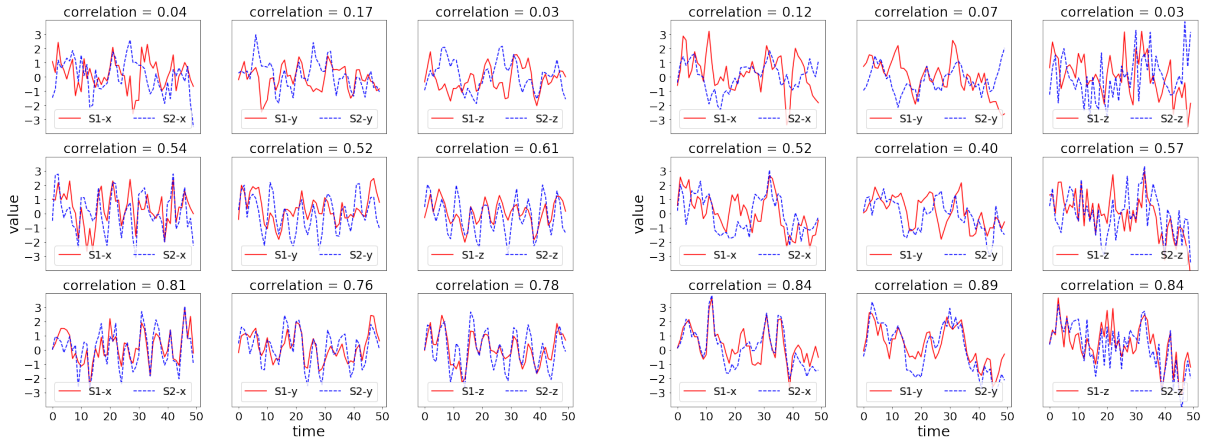


Fig. 12. Sample examples of the synthetic five-class dataset used in our controlled experiments. The nine plots on the left are samples of class 0, and those at the right are samples of class 4. We consider two sensors S1 and S2 in three settings with average Pearson correlation (computed on the corresponding training dataset for each setting): $0.15 \pm .10$ (as the low correlation setting, plots in the top row), $0.54 \pm .11$ (as the moderate correlation setting, plots in the middle row), and $0.82 \pm .05$ (as the high correlation setting, plots in the bottom row). The Pearson correlation coefficient for each sample is shown at the top of each plot.

rate, in both baseline approaches, we up-sample the received data to 50Hz; as the original (non-adaptive) model is trained for this sampling rate. Fig. 13 shows the average classification accuracy for each model in different settings and three scenarios when the model receives data from both sensors S1 and S2, or only from one of them. In Fig. 14 we show the average performance (among all three scenarios of receiving data from both sensors S1 and S2, or only from one of them) presented separately for each class. Our findings are as follows:

First, Fig. 13 shows that when both sensors are available and the sampling rate is 50Hz, the original model achieves a near 100% accuracy in all three settings; which is expected as our synthetic data is not too complex. However, while in this situation, DANA achieves a performance similar to the original model in the moderate and high correlation setting, for the low correlation setting we observe a fall in the accuracy. Looking at Fig. 14, where we plot the average results per each class, we see that this fall in DANA's accuracy is due to the poor performance for class 0 and class 1. This shows that in situations where there is a low correlation between sensors, DANA cannot easily offer performance similar to the original model.

Second, the correlation between two sensors plays an important role, as we see that both the original and DANA models perform better when there are such correlations. However, the correlation is much more important to DANA than the original model. Interestingly, we see that even a moderate correlation can be very helpful to DANA, as we see that DANA can take advantage of correlation in the data very well in the moderated and high correlation settings. Correlation also helps baseline methods, as we see that in the low correlation setting, the copying data of one sensor is worse than just using the mean values. But in the setting of high correlation, we can get much better results by copying the data of the available sensor than just using the mean value of training data. Interestingly, when the correlation is moderate, these two approaches are almost the same.

Third, we see that the variance in DANA is negligible in Fig. 13, but baseline approaches show much higher variance, especially for situations of missing a sensor. Notice that on average, DANA works much better than the original model, even for the low correlation setting. In addition, Fig. 14 shows that when there is a moderate or high correlation, DANA shows better performance in terms of similarity between different classes. However,

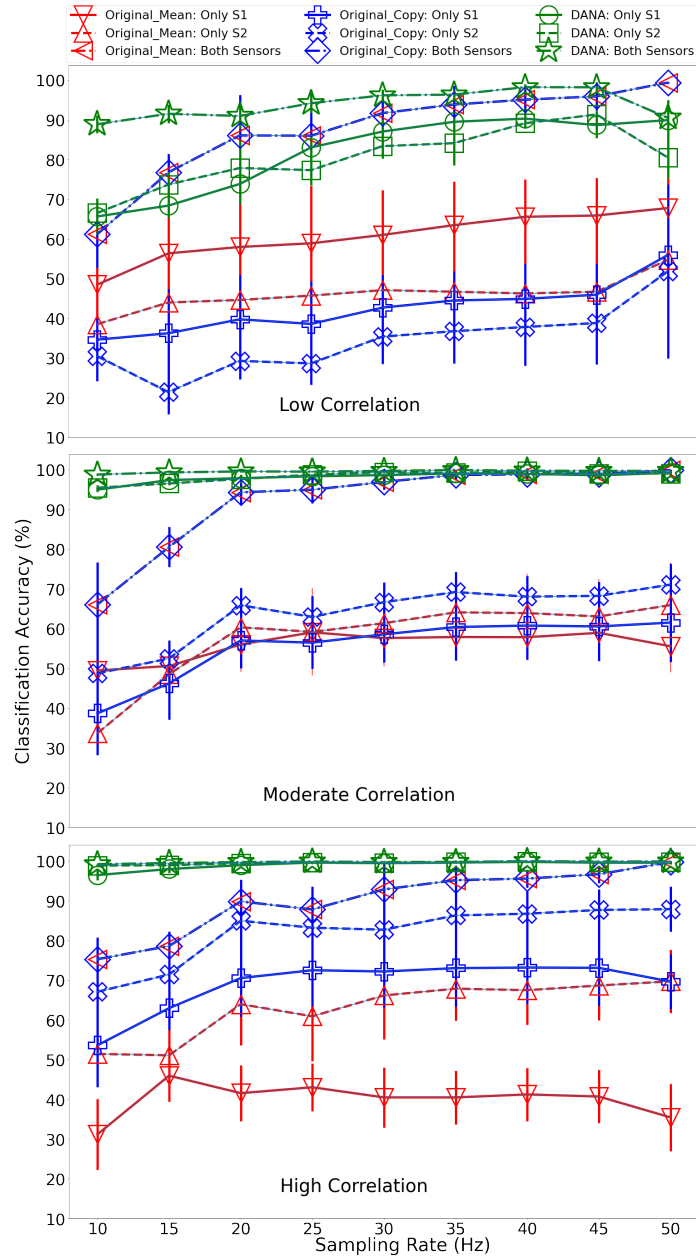


Fig. 13. Comparing DANA with original model on the synthetic dataset in three different settings: (top) *low* correlation, (middle) *moderate*, and (bottom) *high* correlation. Original_Mean means imputing mean values for the sensor that is not available. Original_Copy means duplicating the data of the available sensor for the sensor that is not available.

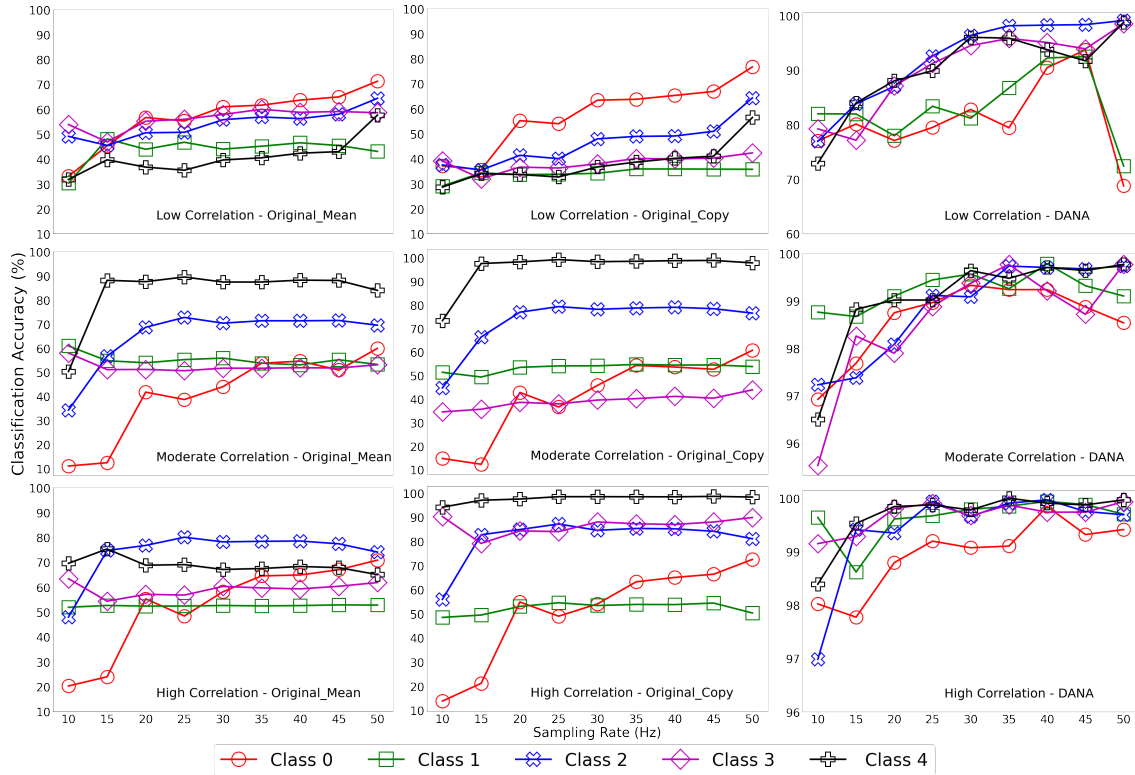


Fig. 14. The average classification accuracy (per each class in the dataset) of three scenarios of receiving data from both sensors S1 and S2, or only from one of them.

the original model shows very different results for each class. We believe this is due to the better generalization capability of DANA, as we also observed in our experiments presented on real-world datasets.

Finally, in this experiment, the concept of correlations between patterns in sensor data is not necessarily restricted to the different sensors of the same device. In general, we can also consider the correlations between the same sensors of different devices. For instance, wearable devices for monitoring people’s health conditions might include sensors at different locations of the user’s body. Since all sensors share a common source of pattern generation (*i.e.* the user’s), their data should have meaningful correlations. However, as our results throughout this paper have shown, when DNNs have not encountered sufficient variability in their input dimensions, they do not capture such correlations and consequently show poor performances when they encounter such variability at inference time. Moreover, it is not intuitive and easy to know what are the underlying rules and correlation patterns between different sensors or different locations. Therefore, another motivation of using DANA, and in general adaptive DNNs, is that they can (based on our experimental observations) capture complex rules in the hierarchy of patterns extracted by the stacked layers in the DNN.

As an example, based on the results in Fig. 13, we observed that if we know how much two sensors are correlated, then we can better choose which imputation technique to apply. Like, if $correlation < C_{low}$ then impute the mean values, and if $correlation > C_{high}$ then impute a copy of available sensors, where C_{low} and C_{high} are two threshold values that can be set based on empirical observations. Readers can immediately notice that

how finding and applying such rules make the task more complicated. On the other hand, we observed that an adaptive model can implicitly find and apply such a rule; showing that by shaping and training a model to be adaptive, we can take better advantage of the capacity of DNNs and capture much more complex rules.

7 DISCUSSION FOR FUTURE STUDIES

In this section, we discuss challenges and new research directions related to DANA and the problem of adaptive sensor and sampling rate selection.

The focus and evaluation of DANA were on motion sensor data. It will be interesting to apply DANA to other types of temporal data, such as audio streams. This needs optimizing the code of the proposed DAP layer for other data types. Moreover, to cover the range of possible data dimensions at inference time, we randomly covered a subset of the possible situations at each round of training DANA. One can study the behavior of this randomized selection alongside the DAT procedure and offer an analysis of the convergence of such training approaches.

An important research direction is also related to measuring the impact of DANA in power saving when running on a wearable or mobile device and the interplay between the operating system of the user's device is an important direction. DANA has applications for situations where users want to control applications' permissions over sensors, which also require research in other areas of such human-computer interactions.

Finally, the majority of public datasets of motion-sensor data do not simultaneously satisfy the requirements of abundance and variety of activities, users, devices, and the number of sensors. Collecting, or getting access to, a larger dataset can help to extend the evaluation of DANA to larger experimental scenarios.

8 CONCLUSION

We presented DANA, a solution to make deep neural networks adaptive to changes in the dimensions of the input data to cope with sensor availability and adaptive sampling at inference time. DANA provides a single trained model that retains high classification accuracy across a range of feasible scenarios, thus avoiding the need for a separate classifier for each setting. Moreover, DANA imposes no limitations to existing DNNs for multivariate sensor data, and it makes DNNs flexible to changes without adding or removing trainable parameters.

We showed that DANA outperforms the state of the art over a range of sampling rates and retains accuracy when some sensors are unavailable at inference time. For instance, on a dataset of 3 sensors and 13 activities, DANA keeps classification accuracy similar to the original DNN in a range of 6Hz to 50Hz and its accuracy only falls from 95% to around 90% and 85% in case of missing one or two of the three sensors, respectively, while the original DNN cannot handle these changes, or achieve at most 75% and 55% accuracy with resampling and imputation preprocessing. Our evaluations on three synthetic datasets have shown that DANA better captures correlated patterns in multi-variate sensor data.

ACKNOWLEDGMENTS

The work was supported by the Life Sciences Initiative at Queen Mary University of London. Mohammad Malekzadeh was partially supported by the UK EPSRC (grant no. EP/T023600/1) within the CHIST-ERA program. Andrea Cavallaro wishes to thank The Alan Turing Institute (EP/N510129/1), which is funded by the EPSRC, for its support through the project PRIMULA. Hamed Haddadi was partially supported by EPSRC Databox: Privacy-Aware Infrastructure for Managing Personal Data (EP/N028260/1) and EPSRC DADA: Defence Against Dark Artefacts (EP/R03351X/1). Authors thank anonymous reviewers for their constructive suggestions provided on the initial version of this paper.

REFERENCES

- [1] Martin Abadi, Paul Barham, Jianmin Chen, Zhifeng Chen, Andy Davis, Jeffrey Dean, Matthieu Devin, Sanjay Ghemawat, Geoffrey Irving, Michael Isard, et al. 2016. Tensorflow: A system for large-scale machine learning. In *12th USENIX Symposium on Operating Systems Design and Implementation (OSDI 16)*. 265–283.
- [2] Mubarak G Abdu-Aguye and Walid Gomaa. 2019. VersaTL: versatile transfer learning for IMU-based activity recognition using convolutional neural networks. In *The 16th International Conference on Informatics in Control, Automation and Robotics (ICINCO)*.
- [3] Jung Ae Lee and Jeff Gill. 2018. Missing value imputation for physical activity data measured by accelerometer. *Statistical methods in medical research* 27, 2 (2018), 490–506.
- [4] Davide Anguita, Alessandro Ghio, Luca Oneto, Xavier Parra, and Jorge Luis Reyes-Ortiz. 2013. A public domain dataset for human activity recognition using smartphones. In *Proceedings of the 21st European Symposium on Artificial Neural Networks, Computational Intelligence and Machine Learning, ESANN*. 437–442.
- [5] Mohamed Ishmael Belghazi, Aristide Baratin, Sai Rajeshwar, Sherjil Ozair, Yoshua Bengio, Aaron Courville, and Devon Hjelm. 2018. Mutual information neural estimation. In *International Conference on Machine Learning*. PMLR, 531–540.
- [6] Yoshua Bengio, Aaron Courville, and Pascal Vincent. 2013. Representation learning: A review and new perspectives. *IEEE transactions on pattern analysis and machine intelligence* 35, 8 (2013), 1798–1828.
- [7] Keith Bonawitz, Hubert Eichner, Wolfgang Grieskamp, Dzmitry Huba, Alex Ingerman, Vladimir Ivanov, Chloe Kiddon, Jakub Konecny, Stefano Mazzocchi, H Brendan McMahan, Timon Van Overveldt, David Petrou, Daniel Ramage, and Jason Roselander. 2019. Towards federated learning at scale: System design. In *Proceedings of the 2nd SysML Conference, Palo Alto, CA, USA*.
- [8] Andreas Bulling, Ulf Blanke, and Bernt Schiele. 2014. A tutorial on human activity recognition using body-worn inertial sensors. *ACM Computing Surveys (CSUR)* 46, 3 (2014), 1–33.
- [9] Zhenyu Chen, Mu Lin, Fanglin Chen, Nicholas D Lane, Giuseppe Cardone, Rui Wang, Tianxing Li, Yiqiang Chen, Tanzeem Choudhury, and Andrew T Campbell. 2013. Unobtrusive sleep monitoring using smartphones. In *7th International Conference on Pervasive Computing Technologies for Healthcare and Workshops (Venice, Italy)*. IEEE, 145–152.
- [10] Weihao Cheng, Sarah Erfani, Rui Zhang, and Ramamohanarao Kotagiri. 2018. Learning datum-wise sampling frequency for energy-efficient human activity recognition. In *Thirty-Second AAAI Conference on Artificial Intelligence*.
- [11] Jun-Ho Choi and Jong-Seok Lee. 2019. EmbraceNet: A robust deep learning architecture for multimodal classification. *Information Fusion* 51 (2019), 259–270.
- [12] Prafulla Kumar Choubey, Shubham Pateria, Aseem Saxena, Vaisakh Punnekkattu Chirayil SB, Krishna Kishor Jha, and Sharana Basaiah PM. 2015. Power efficient, bandwidth optimized and fault tolerant sensor management for IOT in Smart Home. In *2015 IEEE International Advance Computing Conference (IACC)*. IEEE, 366–370.
- [13] David Chu, Nicholas D Lane, Ted Tsung-Te Lai, Cong Pang, Xiangying Meng, Qing Guo, Fan Li, and Feng Zhao. 2011. Balancing energy, latency and accuracy for mobile sensor data classification. In *Proceedings of the 9th ACM Conference on Embedded Networked Sensor Systems*. 54–67.
- [14] Gregory W Corder and Dale I Foreman. 2014. *Nonparametric statistics: A step-by-step approach*. John Wiley & Sons.
- [15] Chelsea Finn, Pieter Abbeel, and Sergey Levine. 2017. Model-agnostic meta-learning for fast adaptation of deep networks. In *Proceedings of the 34th International Conference on Machine Learning-Volume 70*. JMLR. org, 1126–1135.
- [16] Robert M French. 1999. Catastrophic forgetting in connectionist networks. *Trends in cognitive sciences* 3, 4 (1999), 128–135.
- [17] Hassan Ghasemzadeh, Navid Amini, Ramyar Saeedi, and Majid Sarrafzadeh. 2014. Power-aware computing in wearable sensor networks: An optimal feature selection. *IEEE Transactions on Mobile Computing* 14, 4 (2014), 800–812.
- [18] Ian Goodfellow, Yoshua Bengio, Aaron Courville, and Yoshua Bengio. 2016. *Deep learning*. Vol. 1. MIT press Cambridge.
- [19] Dawud Gordon, Jurgen Czerny, Takashi Miyaki, and Michael Beigl. 2012. Energy-efficient activity recognition using prediction. In *2012 16th International Symposium on Wearable Computers*. IEEE, 29–36.
- [20] Katrin Hansel, Romina Poguntke, Hamed Haddadi, Akram Alomainy, and Albrecht Schmidt. 2018. What to put on the user: Sensing technologies for studies and physiology aware systems. In *Proceedings of the 2018 CHI Conference on Human Factors in Computing Systems*. 1–14.
- [21] Kaiming He, Xiangyu Zhang, Shaoqing Ren, and Jian Sun. 2015. Spatial pyramid pooling in deep convolutional networks for visual recognition. *IEEE transactions on pattern analysis and machine intelligence* 37, 9 (2015), 1904–1916.
- [22] Sepp Hochreiter and Jurgen Schmidhuber. 1997. Long short-term memory. *Neural computation* 9, 8 (1997), 1735–1780.
- [23] JL Hounslow, LR Brewster, KO Lear, TL Guttridge, R Daly, NM Whitney, and AC Gleiss. 2019. Assessing the effects of sampling frequency on behavioural classification of accelerometer data. *Journal of experimental marine biology and ecology* 512 (2019), 22–30.
- [24] Hui-Huang Hsu, Chin-Ting Chu, Yinghui Zhou, and Zixue Cheng. 2015. Two-phase activity recognition with smartphone sensors. In *2015 18th International Conference on Network-Based Information Systems*. IEEE, 611–615.
- [25] Andrey Ignatov. 2018. Real-time human activity recognition from accelerometer data using Convolutional Neural Networks. *Applied Soft Computing* 62 (2018), 915–922.

- [26] Jeya Vikranth Jeyakumar, Liangzhen Lai, Naveen Suda, and Mani Srivastava. 2019. SenseHAR: a robust virtual activity sensor for smartphones and wearables. In *Proceedings of the 17th Conference on Embedded Networked Sensor Systems*. 15–28.
- [27] Fazle Karim, Somshubra Majumdar, Houshang Darabi, and Shun Chen. 2017. LSTM fully convolutional networks for time series classification. *IEEE access* 6 (2017), 1662–1669.
- [28] Kleomenis Katevas, Ilias Leontiadis, Martin Pielot, and Joan Serra. 2017. Practical processing of mobile sensor data for continual deep learning predictions. In *Proceedings of the 1st International Workshop on Deep Learning for mobile systems and applications*. 19–24.
- [29] Osman Semih Kayhan and Jan C van Gemert. 2020. On translation invariance in cnns: Convolutional layers can exploit absolute spatial location. In *Proceedings of the IEEE/CVF Conference on Computer Vision and Pattern Recognition*. 14274–14285.
- [30] Aftab Khan, Nils Hammerla, Sebastian Mellor, and Thomas Plotz. 2016. Optimising sampling rates for accelerometer-based human activity recognition. *Pattern Recognition Letters* 73 (2016), 33–40.
- [31] Diederik P Kingma and Jimmy Ba. 2014. Adam: A method for stochastic optimization. In *Proceedings of the 3rd International Conference on Learning Representations (ICLR)*.
- [32] Lukas Koping, Kimiaki Shirahama, and Marcin Grzegorzec. 2018. A general framework for sensor-based human activity recognition. *Computers in biology and medicine* 95 (2018), 248–260.
- [33] Yann LeCun and Yoshua Bengio. 1995. Convolutional networks for images, speech, and time series. *The handbook of brain theory and neural networks* 3361, 10 (1995), 1995.
- [34] Yann LeCun, Yoshua Bengio, and Geoffrey Hinton. 2015. Deep learning. *nature* 521, 7553 (2015), 436–444.
- [35] Yunji Liang, Xingshe Zhou, Zhiwen Yu, and Bin Guo. 2014. Energy-efficient motion related activity recognition on mobile devices for pervasive healthcare. *Mobile Networks and Applications* 19, 3 (2014), 303–317.
- [36] Min Lin, Qiang Chen, and Shuicheng Yan. 2014. Network In Network. In *Proceedings of the 2nd International Conference on Learning Representations, ICLR*.
- [37] Jonathan Long, Evan Shelhamer, and Trevor Darrell. 2015. Fully convolutional networks for semantic segmentation. In *Proceedings of the IEEE conference on computer vision and pattern recognition*. 3431–3440.
- [38] Mohammad Malekzadeh, Richard G. Clegg, Andrea Cavallaro, and Hamed Haddadi. 2018. Protecting Sensory Data Against Sensitive Inferences. In *Proceedings of the 1st Workshop on Privacy by Design in Distributed Systems (Porto, Portugal) (W-P2DS18)*. ACM, Article 2, 6 pages.
- [39] Mohammad Malekzadeh, Richard G. Clegg, Andrea Cavallaro, and Hamed Haddadi. 2019. Mobile Sensor Data Anonymization. In *Proceedings of the International Conference on Internet of Things Design and Implementation (IoTDI) (Montreal, Quebec, Canada)*. ACM, 49–58.
- [40] Mohammad Malekzadeh, Richard G Clegg, Andrea Cavallaro, and Hamed Haddadi. 2020. Privacy and Utility Preserving Sensor-Data Transformations. *Pervasive and Mobile Computing* (2020).
- [41] Akhil Mathur, Anton Isopoussu, Nadia Berthouze, Nicholas D Lane, and Fahim Kawsar. 2019. Unsupervised domain adaptation for robust sensory systems. In *Adjunct Proceedings of the 2019 ACM International Joint Conference on Pervasive and Ubiquitous Computing and Proceedings of the 2019 ACM International Symposium on Wearable Computers*. 505–509.
- [42] David C Mohr, Mi Zhang, and Stephen M Schueller. 2017. Personal sensing: understanding mental health using ubiquitous sensors and machine learning. *Annual review of clinical psychology* 13 (2017), 23–47.
- [43] Yunyoung Nam, Yeesock Kim, and Jinseok Lee. 2016. Sleep monitoring based on a tri-axial accelerometer and a pressure sensor. *Sensors* 16, 5 (2016), 750.
- [44] Alex Nichol, Joshua Achiam, and John Schulman. 2018. On first-order meta-learning algorithms. *arXiv preprint arXiv:1803.02999* (2018).
- [45] Francisco Ordonez and Daniel Roggen. 2016. Deep convolutional and LSTM recurrent neural networks for multimodal wearable activity recognition. *Sensors* 16, 1 (2016), 115.
- [46] Ben Poole, Sherjil Ozair, Aaron Van Den Oord, Alex Alemi, and George Tucker. 2019. On variational bounds of mutual information. In *International Conference on Machine Learning*. PMLR, 5171–5180.
- [47] Xin Qi, Matthew Keally, Gang Zhou, Yantao Li, and Zhen Ren. 2013. AdaSense: Adapting sampling rates for activity recognition in body sensor networks. In *2013 IEEE 19th Real-Time and Embedded Technology and Applications Symposium (RTAS)*. IEEE, 163–172.
- [48] Ning Qian. 1999. On the momentum term in gradient descent learning algorithms. *Neural networks* 12, 1 (1999), 145–151.
- [49] Erwin Quiring, David Klein, Daniel Arp, Martin Johns, and Konrad Rieck. 2020. Adversarial Preprocessing: Understanding and Preventing Image-Scaling Attacks in Machine Learning. In *29th USENIX Security Symposium (USENIX Security 20)*. USENIX Association, 1363–1380.
- [50] Andrew Raij, Animikh Ghosh, Santosh Kumar, and Mani Srivastava. 2011. Privacy risks emerging from the adoption of innocuous wearable sensors in the mobile environment. In *Proceedings of the SIGCHI Conference on Human Factors in Computing Systems*. 11–20.
- [51] Erik Reinertsen and Gari D Clifford. 2018. A review of physiological and behavioral monitoring with digital sensors for neuropsychiatric illnesses. *Physiological measurement* 39, 5 (2018), 05TR01.
- [52] Sebastien Richo, Lin Wang, Philip Birch, and Daniel Roggen. 2020. Transportation mode recognition fusing wearable motion, sound and vision sensors. *IEEE Sensors Journal* (2020).

- [53] Charissa Ann Ronao and Sung-Bae Cho. 2016. Human activity recognition with smartphone sensors using deep learning neural networks. *Expert systems with applications* 59 (2016), 235–244.
- [54] Sara Saeedi and Naser El-Sheimy. 2015. Activity recognition using fusion of low-cost sensors on a smartphone for mobile navigation application. *Micromachines* 6, 8 (2015), 1100–1134.
- [55] Jurgen Schmidhuber. 2015. Deep learning in neural networks: An overview. *Neural networks* 61 (2015), 85–117.
- [56] Emily LC Shepard, Rory P Wilson, Lewis G Halsey, Flavio Quintana, Agustina Gomez Laich, Adrian C Gleiss, Nikolai Liebsch, Andrew E Myers, and Brad Norman. 2008. Derivation of body motion via appropriate smoothing of acceleration data. *Aquatic Biology* 4, 3 (2008), 235–241.
- [57] Muhammad Shoaib, Stephan Bosch, Ozlem Durmaz Incel, Hans Scholten, and Paul JM Havinga. 2016. Complex human activity recognition using smartphone and wrist-worn motion sensors. *Sensors* 16, 4 (2016), 426.
- [58] Robert H Shumway, David S Stoffer, and David S Stoffer. 2000. *Time series analysis and its applications*. Vol. 3. Springer.
- [59] Nitish Srivastava, Geoffrey Hinton, Alex Krizhevsky, Ilya Sutskever, and Ruslan Salakhutdinov. 2014. Dropout: a simple way to prevent neural networks from overfitting. *The journal of machine learning research* 15, 1 (2014), 1929–1958.
- [60] Tijmen Tieleman and Geoffrey Hinton. 2012. Lecture 6.5-rmsprop: Divide the gradient by a running average of its recent magnitude. *COURSERA: Neural networks for machine learning* 4, 2 (2012), 26–31.
- [61] George Vavoulas, Charikleia Chatzaki, Thodoris Malliotakis, Matthew Pedititis, and Manolis Tsiknakis. 2016. The MobiAct Dataset: Recognition of Activities of Daily Living using Smartphones.. In *ICT4AgeingWell*. 143–151.
- [62] Emily Walton, Christy Casey, Jurgen Mitsch, Jorge A Vazquez-Diosdado, Juan Yan, Tania Dottorini, Keith A Ellis, Anthony Winterlich, and Jasmeet Kaler. 2018. Evaluation of sampling frequency, window size and sensor position for classification of sheep behaviour. *Royal Society open science* 5, 2 (2018), 171442.
- [63] Jindong Wang, Yiqiang Chen, Shuji Hao, Xiaohui Peng, and Lisha Hu. 2019. Deep learning for sensor-based activity recognition: A survey. *Pattern Recognition Letters* 119 (2019), 3–11.
- [64] Rui Wang, Min S. H. Aung, Saeed Abdullah, Rachel Brian, Andrew T. Campbell, Tanzeem Choudhury, Marta Hauser, John Kane, Michael Merrill, Emily A. Scherer, Vincent W. S. Tseng, and Dror Ben-Zeev. 2016. CrossCheck: Toward Passive Sensing and Detection of Mental Health Changes in People with Schizophrenia. In *Proceedings of the 2016 ACM International Joint Conference on Pervasive and Ubiquitous Computing* (Heidelberg, Germany). ACM, 886–897.
- [65] Yichong Xu, Tianjun Xiao, Jiaying Zhang, Kuiyuan Yang, and Zheng Zhang. 2015. Scale-invariant convolutional neural networks. In *Proceedings of the IEEE conference on computer vision and pattern recognition*.
- [66] Zhixian Yan, Vigneshwaran Subbaraju, Dipanjan Chakraborty, Archan Misra, and Karl Aberer. 2012. Energy-efficient continuous activity recognition on mobile phones: An activity-adaptive approach. In *2012 16th international symposium on wearable computers*. IEEE, 17–24.
- [67] Jianbo Yang, Minh Nhut Nguyen, Phyo Phyo San, Xiao Li Li, and Shonali Krishnaswamy. 2015. Deep convolutional neural networks on multichannel time series for human activity recognition. In *Twenty-Fourth International Joint Conference on Artificial Intelligence*.
- [68] Xiaodong Yang, Yiqiang Chen, Hanchao Yu, Yingwei Zhang, Wang Lu, and Ruizhe Sun. 2020. Instance-Wise Dynamic Sensor Selection for Human Activity Recognition. In *Proceedings of the AAAI Conference on Artificial Intelligence*, Vol. 34. 1104–1111.
- [69] Shuochao Yao, Shaohan Hu, Yiran Zhao, Aston Zhang, and Tarek Abdelzaher. 2017. Deepsense: A unified deep learning framework for time-series mobile sensing data processing. In *Proceedings of the 26th International Conference on World Wide Web*. 351–360.
- [70] Piero Zappi, Clemens Lombriser, Thomas Stiefmeier, Elisabetta Farella, Daniel Roggen, Luca Benini, and Gerhard Troster. 2008. Activity recognition from on-body sensors: accuracy-power trade-off by dynamic sensor selection. In *European Conference on Wireless Sensor Networks*. Springer, 17–33.
- [71] Hengshuang Zhao, Jianping Shi, Xiaojuan Qi, Xiaogang Wang, and Jiaya Jia. 2017. Pyramid scene parsing network. In *Proceedings of the IEEE conference on computer vision and pattern recognition*. 2881–2890.
- [72] Yu Zhao, Rennong Yang, Guillaume Chevalier, Ximeng Xu, and Zhenxing Zhang. 2018. Deep residual bidir-LSTM for human activity recognition using wearable sensors. *Mathematical Problems in Engineering* 2018 (2018).
- [73] Xiaojun Zhu, Qun Li, and Guihai Chen. 2013. APT: Accurate outdoor pedestrian tracking with smartphones. In *2013 Proceedings IEEE INFOCOM*. IEEE, 2508–2516.